Manuscript Number:	ejm150060R1
Article Type:	Research paper
Full Title:	Continuous dehydration of cavansite under dynamic conditions by in situ synchrotron powder diffraction
Short Title:	"Dehydration of cavansite under dynamic conditions "
Corresponding Author:	Annalisa Martucci, Ph.D. University of Ferrara Ferrara, ITALY
Corresponding Author E-Mail:	mrs@unife.it
Order of Authors:	Annalisa Martucci, Ph.D.
	Elisa Rodeghero
	Giuseppe Cruciani
Abstract:	The dehydration dynamics of cavansite, $Ca(VO)(Si_4O_{10})*4H_2O$ was studied by time-resolved in situ synchrotron powder diffraction between 298 and 900 K. The crystal structure evolution was continuously monitored through 20 Rietveld structure refinements (Pnma space group) in the 298-810 K range whereupon cavansite turned amorphous without any precursor to a polymorphic phase transition to pentagonite. The results achieved from the series of time-resolved Rietveld refinements allowed to highlight the out-of-equilibrium effects which govern dehydration of cavansite powders in dynamic conditions. While confirming the general picture of cavansite dehydration, as previously reported by static single crystal work, our dynamic study discovered the occurrence of an important transient phenomenon which is the cell volume expansion caused by framework relaxation resulting from breakdown of the hydrogen bonding network in the initial heating stages. We also documented that the channels formed by elliptical eight-membered tetrahedral rings of cavansite, when heated under the typical dynamic conditions of an industrial process, undergo a series of short-lived "breathing" pulses which could be exploited for fine tuning of gas diffusion paths in possible applications of synthetic analogues of these vanadosilicates.
Keywords:	cavansite, dehydration dynamics, in situ synchrotron powder diffraction, transient phenomena, framework breathing effect.
Manuscript Region of Origin:	ITALY
Requested Editor:	Sergey V. Krivovichev
Additional Information:	
Question	Response
Author Comments:	Dear Editor, We wish to submit the revised version of our ms. ejm150060. to special issue of the European Journal of Mineralogy, to honor Thomas Armbruster. In order to account for the criticism in particular of Reviewer #1 we have checked all refinements and fully rewritten the paper trying to convey the novelty and reliability of our results in a more effective way. We are firmly convinced about the high quality of our synchrotron data and we did our best to show the our results fully deserve to appear on the EJM special issue to honor Prof. Armbruster. We assure you that this manuscript has not been previously published elsewhere.
Response to Reviewers:	Reply to Referees' comments on paper by Martucci et al. submitted to EJM (Special

issue to honor Thomas Armbruster) - Ref.: ejm150060

Old title: "Dehydration dynamics of cavansite probed by in situ synchrotron powder diffraction"

New title: "Continuous dehydration of cavansite under dynamic conditions by in situ synchrotron powder diffraction"

Comments by Referee #1

The paper "Dehydration dynamics of cavansite probed by in situ synchrotron powder diffraction" by Martucci A., Rodeghero E. and Cruciani G. uses full-profile Rietveld refinements to study unit-cell and crystal structure modification upon dehydration of cavansite. However, the manuscript lacks originality and aim and it is also sloppy prepared (1). The paper should be rejected because the quality of the synchrotron data is by far not sufficient (2) to allow any comparison with X-ray single-crystal data of a very recent paper by Danisi et al. (2012). In addition, if the authors aim in their manuscript for kinetic aspects of dehydration of cavansite, experiments with only a single heating rate (3) of 5K/min are insufficient for a meaningful interpretation.

In general, temperature dependent powder synchrotron diffraction is a useful method to track dehydration of a zeolite if single crystals are not available or kinetic aspects are systematically investigated. However, in case of cavansite such an approach is not useful because temperature dependent X-ray data have previously demonstrated (Danisi et al., 2012) that at elevated temperature the H_2O distribution is strongly disordered.
The limited spatial resolution of powder synchrotron data (2) does obviously not allow to detect or to model such disordered arrangements.
This can be easily demonstrated by a comparison with the thermogravimetric data shown by the authors. Their Fig. 2 indicates that up to 398K 1 H_2O is expelled (1 H_2O corresponds to ca. 4 wt.%). The second H_2O molecule is released up to 518K, the third one up to 677K and the last one essentially at ca. 800K. In addition, their DTG results indicate that there are at least 5 well defined dehydration steps (398, 516, 610, 720, 768K). This discrepancy to the synchrotron data is not discussed. (4)

The problem of dehydration and H_2O distribution in cavansite can also be tackled from a crystallographic point of view: At RT there are three H_2O sites, two at a special position (O8, O9) accounting 1 H_2O pfu each, and one at a general position (O7) accounting 2 H_2O pfu. How can 3 H_2O sites produce 5 dehydration steps? The answer to this question is provided by Danisi et al. (2012) but ignored in the present synchrotron study. (4)

The motivation of the study by Danisi et al. (2012) was the problem of release of H_2O from the O9 site, which has the longest distance to Ca (ca. 2.8 Å). Rinaldi et al. (1975) reported that a H_2O molecule corresponding to the O9 site survives heating at 350°C under vacuum. How can this be explained? Stepwise (25°C) dehydration experiments under dry conditions by Danisi et al. (2012) demonstrated that O9 is already released at 75°C as expected from the weak bonding to Ca and framework O. With release of H_2O at O9, the additional H_2O site O7 becomes strongly disordered partly covering the position of previous O9. The electron cloud due to H_2O disorder around Ca adopts an umbrella-like appearance, modeled by Danisi et al. (2012) by three subsites (O7, O7a, O7b) which are further multiplied by the mirror plane perpendicular to b. Thus, in the single crystal structure refinement this disorder was modeled by six closely spaced positions.(5) With decrease of occupation of these O7 subsites, the umbrella reduces size (it continuously "closes") and the remaining O7 subsites occupy positions close to the mirror plane. This arrangement was interpreted by Rinaldi et al. (1975) as O9 site on the mirror plane with strongly anisotropic displacement parameters. Above 175°C (Danisi et al. 2012) the sum of O7 subsites can only be ½ occupied due to the short separation perpendicular to the mirror plane. Thus, O7 loses H_2O in 2 steps. All the above results were in fact described but also ignored in the refinement strategy by Martucci et al.(5)

The obvious differences to the results of Danisi et al. (2012) were simply assigned to

kinetic variation.(5)

Martucci et al. describe a 3 step dehydration of O9 becoming vacant only at 675K. Their O7 site, modeled as single site with isotropic displacement parameter, which is not acceptable considering the strong disorder (5) seen in the single-crystal data, shows a tendency (Fig. 7) of two-step dehydration. However, below 675K O7 is shown to host 1.2 H2O pfu and O9 additional 0.3 H2O. I would suspect that O9 is a subsite of O7 and that the short separation between these sites does not allow occupation of in total 1.5 H2O pfu. Unfortunately, this aspect cannot be checked because results of structure refinements in this most interesting temperature range are not shown by the authors. Martucci et al. discuss dehydration steps at 406, 514 and 594 K without providing the refinement results. (6)

 "No water splitting was observed but the dehydration occurred with a continuous and gradual release of water
molecules at temperatures different from those reported by Danisi et al. (2012)".

I doubt whether powder refinements are suitable to resolve closely spaced subsites. Thus the method is not appropriate for such complex and disordered H2O arrangements. (2)(5)

Furthermore, their coordinates at 783K (768K in Fig. 7) do not correspond (Table 4SI) with the drawing (7) shown in Fig. 3d. This is not simply due to a single typo! Si1-O distances are between 1.78 and 2.26 Å. Some T-O-T angles are close to 90° and O-O distances are commonly around 2 Å (O4-O5 even 1.6 Å). Fig 3d, 783K, (center) is the same as Fig. 3a center at RT. At least the H2O sites should be labeled for better understanding the dehydration. (8) T-O5-T angles in Fig. 8 above 700K are shown between 110 and 115°. Such highly unusual values require at least comment. (9)

In summary, not only the H2O occupancies but also some framework refinements appear partly unreliable.

In the discussion section, the authors are not convincing with their arguments and I will indicate some critical points.

"It has been recognized that several factors concur to strictly control the thermal behavior of microporous
materials (Cruciani, 2006; Alberti and Martucci 2011; Alberti, A Martucci, 2005; Arletti et al., 2006) the
interplay among these factors being still matter of investigation. Different experimental procedures of the
heating and data collection processes (e.g. single crystal vs. powder diffraction, "ex situ" vs. "in situ" heating,
"at-equilibrium" vs. "far-from-equilibrium" conditions) can also lead to a different the response of a given
microporours material".

I fully share the opinion of the authors. Nevertheless, there are recent papers (Wang & Bish (2012); Cametti et al. (2015); Schmidmair et al. (2015)) showing that different PH2O conditions can significantly influence the dehydration behavior of zeolites. In 2015, the authors cannot ignore this crucial parameter while performing the experiment. The PH2O must be monitored. (10)

To demonstrate the difference between a stepwise in situ dehydration under dry conditions (single-crystal data) with continuous in situ measurements by synchrotron powder diffraction at least the cell volumes and the corresponding H2O content at each plateau of constant volume could have been shown and discussed for the two data sets. I have sketched such a plot (see below). One would expect that independent of the experimental conditions, a similar volume corresponds to a similar H2O content. (11) This seems not to be the case, which may be due low quality of a temperature dependent powder refinement concerning strongly disordered H2O sites in cavansite. If similar unit-cell volumes (single-crystal experiment (pseudo-equilibrium) vs. "dynamic" powder diffraction data) correspond to different H2O content due to kinetic reasons, a discussion or interpretation is a requisite. (11) However, as mentioned

above, with only one heating rate for the "dynamic" powder data such results remain rather puzzling. In this sense the manuscript just opens questions without offering answers. Why does in their data the volume decrease at several points but the H2O content remains essentially the same? (11)

[referee's Figure omitted for clarity]

There are many minor problems (12) (e.g., Ref. Danisi et al. 2014 missing, Danisi et al. 2015 in references but not cited in the text, the style of reference is often not in agreement with the guidelines for authors (EJM); the sentence "The powder sample was loaded and packed in a 0.3 mmm diameter Lindemann capillary, open at both ends, and heated in situ using a hot air stream" is repeated twice in the experimental part). I do not refer to additional minor points in the text because with the presented data the manuscript cannot be recommended for publication in EJM. It is even my firm conviction that this manuscript cannot be improved on the basis of the existing data. (2)

Reply to comments by Referee #1

(1)"lacks originality and aim and it is also sloppy prepared"
Following the Referee's criticism we have carefully checked our results and fully rewritten the manuscript, clearly stating our aims and highlighting our original findings.
Excerpt from new "Introduction":
In spite of the very detailed picture on the static dehydration process of cavansite provided by the accurate single crystal study of Danisi et al. (2012), several open issues still remain for a complete understanding of cavansite thermal behaviour under dynamic conditions. First of all, in order to explain the nearly continuous (at variance with the step-like, as found by Danisi et al. 2012) water loss up to 720K, observed from the TG/DTA curves of cavansite by Ishida et al. (2009), the structural XRD investigation should match the same conditions (kinetic regime, heating rate, atmosphere) and sample (i.e. same composition and crystal size) as in the thermal analyses. Secondly, a vast literature has proved that unpredictable transient structural states might occur in zeolite-like structures such as the "breathing effect" in which a relaxation of hydrogen bonding interactions during the initial heating stages or the diffusion of water molecules through the zeolite-like channels cause the tetrahedral rings to dynamically change from close and distorted, to wide and regular, to close and wrapped again. These dynamic "out-of-equilibrium" structural effects are of fundamental importance to correctly explain phenomena such as the negative thermal expansion or the hindered ("trap door") diffusion effects which often play a role in the technological applications of zeolite-like materials. Single-crystal experiments are not suited to detect transient out-of-equilibrium effects because the relatively long acquisition time of a single snapshot requires that the structure has reached as much as possible a steady state ("near-equilibrium" condition). A third issue is the possible occurrence of the phase transition, as suggested by Evans (1973) and Ishida et al. (2009), from cavansite to pentagonite upon full dehydration at T > 720K. It is noteworthy that gismondine, $CaAl_2Si_2O_8 \cdot 4H_2O$, whose crystal structure is very similar to that of cavansite, when dehydrated in dynamic conditions exhibits three major phase transitions (Milazzo et al. 1998).
In order to shed more light on the above issues and achieve a complete and continuous picture of the cavansite dehydration process under dynamic conditions, in this work we performed an in situ high-temperature (HT) synchrotron X-ray powder diffraction (XRPD) experiment and a series of full Rietveld structural refinements, using the same heating conditions of the TG/DTA curves measured on a polycrystalline sample from the same specimen.
Excerpt from new "Conclusions":
As the most significant and unique result of our study compared to what previously done, we were able to monitor one important transient phenomenon of the type that can only be detected under dynamic out-of-equilibrium conditions. This phenomenon is the cell volume expanding framework relaxation in the initial heating stages which resulted from breakdown of the firmly cross-linked hydrogen bonding system nicely described at RT by Danisi et al. (2012). This phenomenon brought about a short-lived "breathing" of the cavansite framework which is a dynamic effect typical of many zeolite-like flexible network structures. This kind of effects are regarded with much interest because they can be exploited in applications, such as gas separation, for fine tuning of zeolite channel apertures or for engineering of kinetically hindered

mechanisms such as the "trap door" effect (Reisner et al. 2000). Figure 5 clearly shows that under the dynamic heating conditions of a possible industrial application cavansite exhibits a clear cross-over temperature (~550K) below which the its framework undergoes "breathing" with three recognizable pulses. Above 550K the transient cell-expanding effect has ended and the framework proceeds to an progressive squashing of eight-ring channels assisted by the counter-rotations around the 4MR-O5-4MR hinges. A similar behaviour was also observed in cavansite under high-pressure conditions (Danisi et al., 2015) when the T-O-T angles antirotate while the V-O-T angles corotate when the volume decrease. We found that the extreme collapse of the elliptical apertures leaving just 1.5 Å a minimum free diameter, along with the reduced Ca coordination in agreement with Danisi et al. (2012), leads to the amorphization of cavansite.

Excerpt from new "Abstract":

While confirming the general picture of cavansite dehydration as previously reported by static single crystal work, our dynamic study discovered the occurrence in cavansite of an important transient phenomenon which is the cell volume expanding framework relaxation resulting from breakdown of the hydrogen bonding network in the initial heating stages. We also documented that the channels formed by elliptical eight-membered tetrahedral rings of cavansite, when heated under the typical dynamic conditions of an industrial process, undergo a series of short-lived "breathing" pulses which could be exploited for fine tuning of gas diffusion paths in possible applications of synthetic analogues of these vanadosilicates.

(2) "quality of the synchrotron data is by far not sufficient"; "limited spatial resolution of powder synchrotron data"; "I doubt whether powder refinements are suitable to resolve closely spaced subsites. Thus the method is not appropriate for such complex and disordered H2O arrangements."; "with the presented data the manuscript cannot be recommended for publication in EJM. It is even my firm conviction that this manuscript cannot be improved on the basis of the existing data. (2)"

We think that here the Referee's opinion is too unforgiving as possibly biased by his/her little experience with synchrotron powder diffraction and Rietveld refinements. While there is no doubt that the intrinsic physical limitation (i.e. the 1D collapse of the 3D r.l.) of powder diffraction makes intensity data less accurate than single xtal XRD data and Rietveld refinements more tricky than single xtal refinements, there is nowadays a universal consensus that the two techniques can profitably complement each other (by allowing completely different experimental conditions, as in our case) and in many cases provide results of similar quality (very useful when single xtals are not available or do not allow to be measured under the desired conditions).

Indeed the quality of our synchrotron powder diffraction data is very high: the reciprocal space (angular) resolution measured by the FWHM of peaks ranged from 0.06° at 5°, to 0.08° at 25°, to 0.115° at 45° 2-theta; our cavansite sample scattered very well the X-rays up to a sin(th)/lambda of about 0.49682 Å-1 (i.e. about 1 Å). These mean that the quality of our synchrotron data is among the highest ever measured with a similar experimental set-up (Debye-Scherrer geometry and a translating-imaging plate detector). Time-resolved powder data with a similar set-up have been collected since long time at the X7b beamline, NSLS, Brookhaven (see works by John Hanson and co-workers, John Parise and co-workers) and at the GILDA beamline, ESRF, Grenoble (papers by Artioli, Gualtieri, Lamberti, Meneghini, Quartieri, and our group, just to mention a few). Much more than one hundred articles have been published on top-rank journal based on data from this experimental set-up, similar data collection conditions and type of studied materials (we can provide a list if required).

If we failed to convey our message to Referee #1 it is certainly not the quality of our experimental data to be blamed.

In our revised manuscript we hope we clearly show why time-resolved powder diffraction is a well suited method for our aims and why it can detect phenomena which cannot be detected by single xtal experiments.

(3) "kinetic aspects of dehydration of cavansite, experiments with only a single heating rate"

Considering the "kinetic aspects" of a process does not necessarily mean that we are quantitatively determining the kinetic parameters of a given reaction or transformation. This latter would clearly require a different experimental approach (e.g. several isothermal runs as a function of time, Avrami-like plots, Arrhenius plot, etc.) which was not the aim of our present work. The principal aim of our work was to detect a possible

different behavior of cavansite when dehydration is performed under dynamic conditions closer to the one used for TG analyses and industrial applications.
To make things more clear we have replaced all (or most) of the "kinetic" with "dynamic".

(4) "DTG results indicate that there are at least 5 well defined dehydration steps (398, 516, 610, 720, 768K). This discrepancy to the synchrotron data is not discussed."; "The answer to this question is provided by Danisi et al. (2012) but ignored in the present synchrotron study."
While revising our work we discovered that the DTG peaks were mistakenly labeled. The correct positions of DTG peaks on thermal curves are: 366K, 485K, 601K, 696K, and 751K. Full description   in the "2.1 Material and thermogravimetric analysis" section of revised manuscript:
Our thermogravimetric curves (TG and DTG) are compared in Figure 1 with the TG curve digitalized from Figure 1a of Ishida et al. (2009) and the DTG curve calculated from this latter. Five DTG peaks can be recognized in our sample: the first three at 366K, 485K, and 601K closely match those calculated with data of Ishida et al. (2009) while the last two at 696K and 751K are shifted at slightly higher temperatures. The respective weight losses (wt %) associated to the above DTG peaks are as follow (values calculated from Ishida et al. (2009) data in parentheses): 4.21 (4.11), 4.11 (4.17), 3.95 (4.01), 1.37 (2.46), 1.73 (1.20). We note that the total weight loss in our sample (15.37 wt%) is about 0.6 wt% less than that expected for the ideal H_2O content of cavansite (15.96 wt%). Comparison with the Ishida et al. (2009) data show that the less H_2O content is mostly due to water lost in the last three dehydration steps. However in both cases the dehydration of cavansite ends at about 780K.
All the five DTG peaks are interpreted as following:
The dehydration of cavansite starts at about 320 K with the onset of water loss from the O9 site. Release from this site seems at stop ~410 K whereupon a little water amount (~0.3 H_2O p.f.u.) is kept up to about 500 K. The water release from the O7 site starts at ~430 K and continuously proceeds up to ~670 K, then this site is sharply emptied at ~730 K. The onset of water loss from the O8 site occurs at ~540 K and this site is fully emptied above 750 K. Thus, based on the water site occupancy refinements, the loss of ~0.7 H_2O p.f.u. at O9 is the responsible for the DTG peak at 366 K. The second DTG peak at 485 K is mostly due to release of about 0.8 H_2O p.f.u. from O7 plus the 0.2 residual water at O9. The third DTG peak at 601 K corresponds to the further release of about 0.5 H_2O p.f.u. from O7 combined with the 0.2 water loss at O8. The fourth DTG peak at 696 K is associated to the loss of the residual 0.7 H_2O p.f.u. from O7. The fifth DTG peak at 751K marking the final water loss in cavansite, corresponds to about 0.8 H_2O p.f.u. from the O8 site. The above water losses appear slightly underestimated compared to those calculated from the thermal curves possibly due to correlation of water occupancies and atomic displacement parameters, as noted before. Nevertheless, the water release sequence appears in good agreement with the findings of Danisi et al. (2012), given the discrepancy on the amount of water released in each step.
No discrepancy exist between DTG and XRD data.

(5) "in the single crystal structure refinement this disorder was modeled by six closely spaced positions."; "All the above results were in fact described but also ignored in the refinement strategy by Martucci et al."; "which is not acceptable considering the strong disorder"; "I doubt whether powder refinements are suitable to resolve closely spaced subsites. Thus the method is not appropriate for such complex and disordered H_2O arrangements."
Excerpt from our revised manuscript:
The most significant difference of our results compared those of Danisi et al. (2012) concerns the positional disorder that these authors described for the O7 and O9 water molecules. According to Danisi et al. (2012), the complete release of H_2O from split O9 and O9a sites in the first dehydration step at 348K was accompanied by a splitting of O7 H_2O over three positions O7, O7a, and O7b. These three subsites approached the former O9 position during the next dehydration step at 448K where their sum occupancy decreased to 50%. At 623K, H_2O was expelled from O8 and the residual H_2O at O7 and O7b moved closer to the former O9 site. Further heating to 673K was then assumed to remove the residual water from O7 and O7b and cause the cavansite breakdown. We carefully tested the positional disorder model of Danisi et al. (2012) in our refinement but did not find any evidence for the O9 and O7 split positions. We do

not think that this is due to the limited accuracy of our powder diffraction and Rietveld refinements compared to the single crystal data. Instead we suggest that the different time-frame of our data collection compared to that of Danisi et al. (2012) must be taken into account for a more likely explanation. In our experiment each XRD snapshot collects simultaneously the whole reciprocal lattice in 5 minutes. Each single crystal data collection of Danisi et al. (2012) typically took 480 minutes with 'at least 30 min' annealing time before data collection. We experienced, in our own HT single crystal work, that a too short equilibration time would lead the crystal structure of a zeolite heated in situ to be still changing during a relatively long measurement. Since different portions of the Ewald sphere are typically registered in sequence by CCD images, this would result in an integration of different crystal structure arrangements, changing over the 480 minutes, into a single snapshot. In other words we speculate that the positional disorder found by Danisi et al. (2012) at a given temperature (time) step could actually reflect the overlap of different arrangements of water positions changing in time. As a matter of fact, in their ex situ single crystal work Rinaldi et al. (1975) did not find any evidence for splitting of O7 and W1, the latter being the only water molecule left at 493K in their experimental conditions which they refined with anisotropic displacement parameters. For another possible explanation we note that the much slower diffusion in large (i.e. tenths of millimeter size) single crystals compared to submicrometer size powders make the former very prone to formation of domains with different structural arrangements and cracks due to tensions between domains. The single crystal of Danisi et al. (2012) was broken after the first dehydration step very likely due to internal strain. The occurrence of 10% vanadium pyramids with flipped orientation found ex situ by Rinaldi et al. (1975), but not observed in situ by Danisi et al. (2012), is another sign of possible formation of domains that might be interpreted as disorder. It seems therefore reasonable that, unlike Danisi et al. (2012), we did not observe the split positions for water molecules due to our very different experimental conditions (fast and simultaneous data collection, submicron crystals). Instead, we cannot rule out that the ~0.2 H2O p.f.u. hosted in the O9 site at ~460K (see Figure 7) might have originated from O7 whose water loss had started in the meantime. It is to be noted that the sum of occupancy fractions of O7 and O9 at this temperature is close to 1.0 and is consistent with their short intersite distance (1.87 Å). A similar consideration applies to the partial refilling of ~0.2 H2O the O8 site at ~720K while the occupancy of O7 drops. The occupancy of O7 and O8 at ~720K is acceptable within the error considering the very short distances O7-O8 (1.21 Å) and O7-O7 (1.00 Å) which prevent these water sites to be occupied simultaneously.

In our own HT in situ single xtal work on zeolite dehydration in order to attain the quasi-equilibrium condition at the given temperature we typically keep the crystal overnight (i.e. ~10 hours) before collecting the data at that temperature. In fact, by re-collecting the very first CCD image of data collection at the end we have found that in most cases even a few hours of equilibration time is insufficient. The crystal structure of the dehydrating zeolite at the end of the data collection was different compared to the beginning. The relatively long acquisition time required with single crystal method combined with insufficient equilibration cause an integration of structural states distinct in time into one single data collection. The resolution of single crystal data is superior to powder in the reciprocal space but the time resolution of the former can be a very limiting factor to accurately describe the zeolite dehydration process.

(6) "discuss dehydration steps at 406, 514 and 594 K without providing the refinement results."
The refinement results of the dehydration steps at 433K, 542K, and 783K are now provided as CIF files.

(7) "coordinates at 783K (768K in Fig. 7) do not correspond (Table 4SI) with the drawing"
Typos and mismatches have now been fixed.

(8) "At least the H2O sites should be labeled for better understanding the dehydration."
Labels have been added to Figure 8 (former Figure 3).

(9) "T-O5-T angles in Fig. 8 above 700K are shown between 110 and 115°. Such highly unusual values require at least comment."
The Referee is right, there was a problem here with the last two refinements that we have revised. Now the values of the T1-O5-T2 angle for the last two refinements are

about 125° which is comparable to the 126.1° reported by Rinaldi et al.(1975).
The following sentence has been added in the revised manuscript:
This displacement of the Ca ions induced a sharp increase in the counter-rotation around the O5 oxygens acting as hinges of the four-rings in the plane of the cavansite silicate layers. This counter-rotation was thus responsible for an dramatic squashing of the eight-ring channels delimited by the O5 oxygens (see Figure 8), the Si(1)-O5-Si(2) angle equal to 125° at 810K, leading to a minimum free diameter O5-O5 as low as 1.5 Å (calculated assuming an effective radius of 1.35 Å for oxygen) at 810K. It is conceivable that such an extreme collapse of the channels, hampering the diffusion of the last H_2O molecules leaving the zeolite, caused much instability of the cavansite structure leading to its breakdown.

(10) "In 2015, the authors cannot ignore this crucial parameter while performing the experiment. The PH_2O must be monitored."
We are fully aware of the fundamental dependence of zeolite dehydration dynamics upon the PH_2O. In fact, our aim in the present work was to monitor the dehydration behavior at the same conditions of the TG measurements which are performed as application tests (submicron powder sample, heating in air, open crucible/capillary). Investigating the dehydration behavior while controlling the PH_2O conditions is not a big problem. It simply requires a different experimental approach aimed to tackle an issue which was not among our aims in the present work. The following sentence in the "Introduction" should clarify this point:
...in order to explain the nearly continuous (at variance with the step-like, as found by Danisi et al. 2012) water loss up to 720K, observed from the TG/DTA curves of cavansite by Ishida et al. (2009), the structural XRD investigation should match the same conditions (kinetic regime, heating rate, atmosphere) and sample (i.e. same composition and crystal size) as in the thermal analyses.

Furthermore, one should also consider that the PH_2O dependence of zeolite dehydration is crystal-size dependent too. The assumption that a crystal of tenths of millimeter size is reliable model for the diffusion limited mass (water) transport occurring in submicron crystals (the ones actually used in applications) is a very rough approximation.

(11) "One would expect that independent of the experimental conditions, a similar volume corresponds to a similar H_2O content."; "a discussion or interpretation is a requisite."; "volume decrease at several points but the H_2O content remains essentially the same?"
Excerpt from our revised manuscript:
The variation of the unit cell volume does not follow a trend parallel to the one defined by the water release. In fact , the initial heating stage is accompanied by a clear expansion of the unit cell which stops with the starting of the dehydration. However the first major water release at 366K (DTG peak) is not marked by a sharp drop in the unit cell volume, as it could be expected. Instead, only a minor slope is observed in the 380-420K range. A slight volume contraction is then registered from 420K to about 550K followed by a dramatic contraction of the unit cell volume with a slope centred at about 570K. For T > 590K the overall variation of the unit cell volume is parallel to that of the water release curves. The striking decoupling between water release and cell volume variation in the RT-550K range can be explained by considering the dynamic character and the out-of-equilibrium conditions of our time-resolved experiment. We suggest that the incipient and progressive breakdown of the hydrogen bonding system is responsible for the relaxation and expansion of the cavansite framework which is clearly manifest from RT to 380K but also continues to take place up to about 530K. Thus, in the 380-530K two competing phenomena occur: one is the transient framework expansion related to the hydrogen bonding breakdown, the other is the cell contraction to achieve a volume in equilibrium with the reduced water. The behaviour of the unit cell volume that we have recorded as a function of temperature (and time) is therefore the trade-off between a non-quenchable transient effect and the tendency of the crystal structure to achieve a new equilibrium. If we had let equilibrating our sample at 400K or so and just measure the unit cell volume at the end, we would have missed all the transient phenomena, we would have only measured the contracted cell consistent with the partial dehydration. As a matter of fact this is what has been observed by Danisi et al. (2012) in their static experiment at close-to-equilibrium conditions.

A similar volume corresponds to a similar H2O content only at equilibrium. Transient phenomena and dynamic effects, break down this paradigm. These effects are only detectable by time-resolved out-of-equilibrium experiments.

(12) There are many minor problems
All fixed in the revised manuscript.
Comments by Referee #2

General comments:
This work deals with the structural changes undergone by cavansite during high temperature dehydration and subsequent decomposition, studied by in situ synchrotron powder diffraction between 298 and 900 K.
This topic has been recently investigated by Danisi et al. by single crystal X-ray diffraction and discussed in a detailed paper published in American Mineralogist.
Hence, the results reported here represent a re-visitation of the same scientific problem by means of a different experimental approach and technique.
In my opinion, the ms. deserves publication on EJM especially because it shows and confirms the crucial influence of the kinetic factors in controlling the thermal stability and the structural changes of microporous materials during dehydration.
As a consequence, I suggest the authors to stress more this aspect, both in the Discussion (expanding and detailing the comparative discussion among their results and those of Danisi et al.), and in the Abstract and even in the Title of the paper, that should report explicitly that the paper deals with the importance of the kinetic aspects in the high temperature behavior of cavansite.

Specific comments on the manuscript and the figures:

Most of the specific comments are reported as notes in the merged manuscript pdf file. Open the file and look carefully for the added notes, also in the Figures, Captions and References.

Figures:
Most of the figures are difficult to be read in a B/W version. Please, change the symbols/lines to make them clearer and enlarge the characters, especially those used for the numbers.
The merged manuscript does not contain Fig. SI1. Is this figure equal to Figure 8?

Reply to comments by Referee #2

In the fully rewritten revision of our manuscript we took in due account the Referee's suggestion and extensively emphasized the role of dynamic (kinetic) effects in the HT behavior of cavansite.
The Abstract and Title have been also rewritten accordingly.

All comments by the Referee in the annotated pdf file have been duly accounted for.
Figures have been made more readable, also in B/W version.

Continuous dehydration of cavansite under dynamic conditions by *in situ* synchrotron powder diffraction

A. Martucci, E. Rodeghero and G. Cruciani

Corresponding author:

Annalisa Martucci,

Università degli Studi di Ferrara

Department of Physics and Earth Sciences,

I-44100 - Ferrara

Tel: +39-(0)532-974730

Fax: +39 (0)532-210161

Article layout:

Continuous dehydration of cavansite under dynamic conditions by in situ synchrotron powder diffraction

A. Martucci*, E. Rodeghero and G. Cruciani

Department of Physics and Earth Sciences, University of Ferrara, Via Saragat, 1, I-44122 Ferrara, Italy

* Email: mrs@unife.it

Abstract

The dehydration dynamics of cavansite, $Ca(VO)(Si_4O_{10})•4H_2O$ was studied by time-resolved *in situ* synchrotron powder diffraction between 298 and 900 K. The crystal structure evolution was continuously monitored through 20 Rietveld structure refinements (*Pnma* space group) in the 298-810 K range whereupon cavansite turned amorphous without any precursor to a polymorphic phase transition to pentagonite. The results achieved from the series of time-resolved Rietveld refinements allowed to highlight the out-of-equilibrium effects which govern dehydration of cavansite powders in dynamic conditions. While confirming the general picture of cavansite dehydration, as previously reported by static single crystal work, our dynamic study discovered the occurrence of an important transient phenomenon which is the cell volume expansion caused by framework relaxation resulting from breakdown of the hydrogen bonding network in the initial heating stages. We also documented that the channels formed by elliptical eight-membered tetrahedral rings of cavansite, when heated under the typical dynamic conditions of an industrial process, undergo a series of short-lived "breathing" pulses which could be exploited for fine tuning of gas diffusion paths in possible applications of synthetic analogues of these vanadosilicates.

Keywords: cavansite, dehydration dynamics, *in situ* synchrotron powder diffraction, transient phenomena, framework breathing effect.

1. Introduction

Synthetic microporous vanadosilicates synthesized in the presence of transition metal ions are known to be effectively usable for oxidation chemistry because they contain discrete vanadium centers in the framework that are accessible to molecular and cationic species via the pores. Consequently they can be used in several heterogeneous catalytic reactions such as nitrogen oxides selective catalytic reduction and aromatic hydrocarbons oxidation (Wang et al. 2002; Pietrzyk et al., 2007). In industrial applications these materials are always used as micron- or sub-micron crystal size crystalline powders and their thermal properties are commonly tested by combined thermogravimetric (TG) and differential thermal analysis (DTA) methods. Typical conditions encompass heating in air with temperature ramp rate of 5-10 K/min. However, for a complete understanding of the structural modifications occurring in the material upon heating, a parallel X-ray diffraction analysis performed at the same conditions is required.

Cavansite and its dimorph pentagonite $Ca(VO)(Si_4O_{10}) \cdot 4H_2O$ are the only known natural microporous solids containing stoichiometric amount of vanadium (Danisi et al. 2012; Wang et al., 2002). Recently synthetic VSH-1K and VSH-2Cs are described as open-framework vanadosilicates containing structural motifs similar to cavansite and pentagonite with great potential as molecular sieves or in catalysis due to their high thermal stability and ion-exchange properties (Wang et al., 2002).

The three-dimensional framework of cavansite is built by undulating pyroxenoid-like $(SiO_3)n$ chains having the tetrahedral apices pointing up and down along the **b** axis. (Evans 1973). Adjacent chains are laterally joined into sheets parallel to the **a-c** plane delimited by four-fold and eight-fold rings. These sheets are connected through VO_5 basal square pyramids with the vanadyl group

characterized by a short apical V–O bond (~1.6 Å) and four larger basal bonds (~2.0 Å) (Evans 1973; Solov'ev et al. 1993; Hughes et al. 2011). Differently from cavansite, the network of pentagonite exhibits six-fold tetrahedral rings. A possible reconstructive polymorphic transition from cavansite to pentagonite has been suggested (Evans, 1973), the six-fold rings being favoured at higher temperatures (Ishida et al., 2009). Large cavities of cavansite host in zeolite-like fashion Ca ions eightfold-coordinated to four H_2O molecules and four oxygen atoms of silicate tetrahedra. As accurately shown by Danisi et al. (2012) and detailed afterwards, a cross-linked hydrogen bonding system firmly links the $CaO_4(H_2O)_4$ polyhedron to the framework.

The response to heating of cavansite has been investigated by TG/DTA methods (Ishida et al. 2009 and reference therein), laboratory HT powder diffraction without Rietveld analysis (Ishida et al. 2009), *ex-situ* (Rinaldi et al. 1975) and *in situ* (Danisi et al. 2012) single crystal diffraction, *in-situ* FTIR and Raman spectroscopy (Prasad and Prasad 2007). The high-pressure behaviour has also been studied by Danisi et al. (2015). Rinaldi et al. (1975) determined the crystal structure of partly dehydrated cavansite from Oregon, U.S.A by *ex situ* single crystal XRD. After heating in vacuum at 493 K one water molecule bonded to Ca was found in the structure. The TG/DTA curves measured with heating rate of 10K/min reported by Ishida et al. (2009) for a pure cavansite sample showed a nearly continuous weight loss from RT to about 780 K with five DTG peaks (calculated by us from digitized TG curves in Figure 1a of Ishida et al.) at 369 K, 478 K, 603 K, 678 K and 735 K associated to five DTA endothermic peaks at 368 K, 498 K, 623 K, ~713 K, and 763 K respectively (from Figure 1a of Ishida et al., 2009). The same authors also reported HT powder patterns recorded *in situ* at 293 K, 533 K, 823 K, and 973 K along with the *ex situ* powder pattern after heating at 673 K. Cavansite appeared to preserve its original structure up to 673K while turned amorphous after heating at 823 K. Thus, no conclusive evidence was found to rule out a possible reconstructive phase transition to pentagonite associated to the last dehydration step at 783 K. More recently, Danisi et al. (2012) studied the dehydration behaviour of cavansite by *in situ* single-crystal X-ray diffraction using a relatively large crystal (0.1 x 0.1 x 0.5 mm) and an hot nitrogen stream to

heat the sample. Complete data sets were collected in steps of 25 K up to 523 K and in steps of 50 K up to 673 K. The crystal was kept 30 min at each temperature step before data collection which typically lasted about 8 hours (Rosa Danisi, personal communication). On the basis of the crystal structure refinements a step-like dehydration resulted in 1 H_2O (O9 site) lost at 348 K, 2 H_2O (split O7 positions) lost at 448 K, and 1 H_2O (O8 site) at 623 K, accompanied by a corresponding reduction of Ca coordination from the original eight-fold to seven-, six-, and five-fold, respectively. At 673 K cavansite was no longer crystalline and the lost of the residual water molecule leading to structure breakdown was postulated.

In spite of the very detailed picture on the static dehydration process of cavansite provided by the accurate single crystal study of Danisi et al. (2012), several open issues still remain for a complete understanding of cavansite thermal behaviour under dynamic conditions. Firstly, in order to explain the nearly continuous (at variance with the step-like, as found by Danisi et al., 2012) water loss up to 720 K, observed from the TG/DTA curves of cavansite by Ishida et al. (2009), the structural XRD investigation should match the same conditions (kinetic regime, heating rate, atmosphere) and sample (i.e. same composition and crystal size) as in the thermal analyses. Secondly, a vast literature has proved that unpredictable transient structural states might occur in zeolite-like structures such as the "breathing effect" in which a relaxation of hydrogen bonding interactions during the initial heating stages or the diffusion of water molecules through the zeolite-like channels cause the tetrahedral rings to dynamically change from close and distorted, to wide and regular, to close and wrapped again. These dynamic "out-of-equilibrium" structural effects are of fundamental importance to correctly explain phenomena such as the negative thermal expansion or the hindered ("trap door") diffusion effects which often play a role in the technological applications of zeolite-like materials. Single-crystal experiments are not suited to detect transient out-of-equilibrium effects because the relatively long acquisition time of a single snapshot requires that the structure has reached as much as possible a steady state ("near-equilibrium" condition).

A third issue is the possible occurrence of the phase transition, as suggested by Evans (1973) and Ishida et al. (2009), from cavansite to pentagonite upon full dehydration at T > 720 K. It is noteworthy that gismondine, $CaAl_2Si_2O_8 \cdot 4H_2O$, whose crystal structure is very similar to that of cavansite, when dehydrated in dynamic conditions exhibits three major phase transitions (Milazzo et al. 1998).

In order to shed more light on the above issues and achieve a complete and continuous picture of the cavansite dehydration process under dynamic conditions, in this work we performed an *in situ* high-temperature (HT) synchrotron X-ray powder diffraction (XRPD) experiment and a series of full Rietveld structural refinements, using the same heating conditions of the TG/DTA curves measured on a polycrystalline sample from the same specimen.

2. EXPERIMENTAL

2.1 Material and thermogravimetric analysis

Several crystals of cavansite were handpicked form a specimen from the Wagholi Quarry complex, Poona, India as described by Kothavala (1991) and Makki (2005). Crystals were then reduced in the form of a fine polycrystalline sample by grinding in an agate mortar.

TG/DTA curves on a fraction of the above sample contained in an open alumina crucible were measured in air using a Netzsch STA 409 PC LUXX® simultaneous TG/DTA thermoanalyser. Temperature range and heating rate were from room temperature (RT) to 900 K and 5 K/min, respectively. Our thermogravimetric curves (TG and DTG) are compared in Figure 1 with the TG curve digitalized from Figure 1a of Ishida et al. (2009) and the DTG curve calculated from this latter. Five DTG peaks can be recognized in our sample: the first three at 366 K, 485 K, and 601 K closely match those calculated with data of Ishida et al. (2009) while the last two at 696 K and 751 K are shifted at slightly higher temperatures. The respective weight losses (wt %) associated to the above DTG peaks are as follow (values calculated from Ishida et al. data in parentheses): 4.21 (4.11), 4.11 (4.17), 3.95 (4.01), 1.37 (2.46), 1.73 (1.20). We note that the total weight loss in our

sample (15.37 wt%) is about 0.6 wt% less than that expected for the ideal H_2O content of cavansite (15.96 wt%). Comparison with the Ishida et al. (2009) data shows that the less H_2O content is mostly due to water lost in the last three dehydration steps. However in both cases the dehydration of cavansite ends at about 780 K.

2.2 XRD data collection and Rietveld refinements

 XRD experiments were carried out on the General Italian Line for Diffraction and Absorption (GILDA) beamline at the European Synchrotron Radiation Facility (ESRF) in Grenoble, France. The powder sample was loaded and packed in a 0.3 mm diameter Lindemann capillary, open at both ends, and heated *in situ* using a hot air stream from 298 up to 900 K with a constant heating rate of 5 K/min. In previous work we have found that this sample environment and heating conditions nicely match those used for TG/DTA analysis. Powder diffraction patterns were continuously collected in parallel Debye-Scherrer geometry by a translating imaging plate (TIP) camera (Meneghini et al., 2001), with a fixed wavelength of 0.68765 Å. The parameters of the instrumental setup, namely the sample-to-detector distance, instrumental peak broadening, and IP orthogonality, were calibrated by refining the diffraction patterns of standard LaB_6 reference material. The use of area detectors such as IPs allows diffraction patterns to be collected simultaneously in the wide 2θ range with relatively high counting statistics and reduced acquisition times. The slit delimited portion of the Debye-Scherrer rings, recorded on the IP as a function of temperature, were integrated to the equivalent of a series of 2θ scans using a locally developed computer code. Selected patterns of the *in situ* time-resolved synchrotron X-ray powder diffraction experiment are shown in Figure 2 as a function of temperature.

XRD patterns were analyzed using the Rietveld structural refinement approach as implemented in the General Structure Analysis System (GSAS) package (Larson and Von Dreele, 2000) with the EXPGUI graphical interface (Toby, 2001). Evolution of the crystal structure was observed through 20 structure refinements. The structure refinement at room temperature was performed in the *Pnma*

space group starting from the structural parameters reported by Danisi et al. (2012). The refined structural model was then used as input of the high temperature refinements in the 298 – 810 K temperature range. No evidence was found for any symmetry change up to the highest investigated temperature. The following refinement strategy was used for all refinements. Soft constraints on T-O (1.64 Å) and V-O (1.98 Å) distances were included with a weighting factors gradually reduced up to a final value of F = 50. Difference Fourier maps were repeatedly calculated from the refined model and were used for location of residual electron density corresponding to Ca cations or H_2O molecules. H-atoms were not considered in the structure refinement due to their low X-ray scattering power. The instrumental background was fitted using a Chebyschev polynomial of the first kind with 20 variable coefficients. Peak profiles were modelled by a pseudo-Voigt profile function using Gaussian U, V, and W coefficients, a Lorentzian particle-size broadening term (0.01% cut-off peak intensity). The 2θ-zero shift, scale factor and unit-cell parameters were first refined by modelling the peak intensities through the Le Bail method. In the final cycles, all positional parameters, site occupancy, and isotropic temperature factors were refined. Some refinement details for four selected temperatures (298 K, 433 K, 542 K and 783 K, respectively) are summarized in Table 1 while the corresponding refined atomic parameters are given as Supporting Information (Tables1SI –Tables4SI).

3. RESULTS AND DISCUSSION

3.1 Rietveld refinement of cavansite at RT

The results of our Rietveld refinement of cavansite crystal structure at room temperature are in close agreement to what originally reported by Evans (1973) and more recently by Danisi et al. (2012). In particular, as also found by Evans (1973), the VO$_5$ basal square pyramids show four relatively long V–O bonds (2.008 and 1.975 Å, respectively) on one side of the V atom, and one short one (1.622Å) on the other (average bond length = 1.918 Å). The average bond length of silicate tetrahedra pyroxenoid-like (SiO$_3$)n chains are 1.619 Å and 1.627 Å for Si1 and Si2

tetrahedra, respectively. The Ca–O bond distances, ranging from 2.395 to 2.869 Å (average Ca-O bond length = 2.482 Å), agree closely with those reported by Evans (1973), and Danisi et al. (2012) (average Ca-O bond length = 2.473 Å). Danisi et al. (2012) showed that the hydrogen-bonding system firmly links the extraframework moieties to the framework. In our refinement we evaluated the H$\cdots$O interactions by considering the donor-acceptor (O-O) distances. With reference to the scheme by Danisi et al. (2012), a first H$\cdots$O interaction occurs between the O6 apex of the V square-based pyramid and the H9a hydrogen of the O9 water molecule of the opposing $CaO_4(H_2O)_4$ polyhedron (O9-H9a$\cdots$O6; our refined O9-O6 distance is 2.969 Å). The H9a$\cdots$O6 vector (based on model by Danisi et al., 2012) has the largest component parallel to the **c**-axis and no component along the **b**-axis. A second hydrogen bonding O7-H7b$\cdots$O5 (our refined O7-O5 distance 2.869 Å) together with the weaker interaction O8-H8$\cdots$O3 (refined O8-O3 distance 3.515 Å) link the O7 and O8 water molecules of the Ca coordination shell to the silicate layer. Both the latter interactions have major components along the **a-** and **b-**axis. Finally, the O7-H7a$\cdots$O9 interaction (refined O7-O9 distance 2.860 Å) links together the O7 and O9 water molecules. Our refined D$\cdots$A distances are in perfect agreement with those reported by Danisi et al. (2012) and suggest that the relatively strong and interlinked hydrogen bonding network is likely to exert a significant internal negative pressure on the cavansite channels.

3.3 *In situ* time-resolved analysis

A first overview of the dehydration process in cavansite under dynamic conditions, comparable to those of TG curves, can be gained from Figure 3 in which the variation of the refined unit cell volume is plotted along with the continuous variation of the water contents as obtained from the TG curve and as calculated from the Rietveld refinements. The water content from structure refinements appears slightly overestimated, compared to the thermogravimetric one, possibly due to an overall overestimation of the water molecule atomic displacement parameters. However the trends defined by the two curves are in a perfect agreement. The two major slopes corresponding to

the first two DTG peaks at 366 K and 485 K are clearly visible while the three weight losses at higher temperatures are less marked in both curves. The variation of the unit cell volume does not follow a trend parallel to the one defined by the water release. In fact, the initial heating stage is accompanied by a clear expansion of the unit cell which ends after the starting of the first dehydration step. Remarkably, the first major water release at 366 K (DTG peak) is not marked by a sharp drop in the unit cell volume, as it could be expected. Instead, only a minor slope is observed in the 380-420 K range. A slight volume contraction is then registered from 380 K to about 550 K followed by a dramatic contraction of the unit cell volume with a slope centred at about 570 K. For T > 598 K the overall variation of the unit cell volume follows that of the water release curves. The striking decoupling between water release and cell volume variation in the RT-550 K range can be explained by considering the dynamic character and the out-of-equilibrium conditions of our time-resolved experiment. We suggest that the incipient and progressive breakdown of the hydrogen bonding system is responsible for the relaxation and expansion of the cavansite framework which is clearly manifest from RT to 380 K but also continues to take place up to about 530 K. Thus, in the 380-530 K range two competing phenomena occur: one is the transient framework expansion related to the hydrogen bonding breakdown, the other is the unit cell contraction to achieve a volume in equilibrium with the reduced water content. The behaviour of the unit cell volume that we have recorded as a function of temperature (and time) is therefore the trade-off between a non-quenchable transient effect and the tendency of the crystal structure to achieve a new equilibrium. If we had let equilibrating our sample at 400 K or so and just measured the unit cell volume at the end, we would have missed all the transient phenomena, we would have only measured the contracted cell consistent with the partial dehydration. As a matter of fact this is what has been observed by Danisi et al. (2012) in their static experiment at close-to-equilibrium conditions. The careful examination of the unit cell parameters plotted in Figure 4 as normalized values, $a(T)/a_0$, $b(T)/b_0$, $c(T)/c_0$, and $V(T)/V_0$ with a_0, b_0, c_0, and V_0 being the references refined at 298 K, provides further insights on the breakdown of the hydrogen bonding system. It appears that the lengthening of the **c-**

edge is mostly responsible for the volume expansion up to 380 K suggesting that the weakening of the O9-H$\cdots$O6 interaction which links the apex of the V square-based pyramid and the O9 water molecule of the opposing $CaO_4(H_2O)_4$ polyhedron is the first and most significant. The small lengthening of **b-** and **a-**edges in the 400-520 K range suggests that the release of the interactions involving in particular the O7 water molecule also plays a role in the framework relaxation. Therefore the dramatic volume contraction occurring at 570 K marks the stage in which the net weight loss is no longer counterbalanced by the volume increase due to the framework relaxation. The weakening and breakdown of hydrogen bonding network is known to be the principal reason for relaxation and expansion of zeolite frameworks during the initial heating stages (e.g in hydro-sodalite, Felsche and Luger, 1986; in analcime, Cruciani and Gualtieri, 1999; in wairakite, Seryotkin et al., 2003; in silica sodalite, Leardini et al., 2012; in ZSM-5, Martucci et al., 2015 and Ardit et al., 2015).

The evolution of the O5-O5 distances defining the short and long axes of the elliptically shaped eight-membered tetrahedral rings (Figure 5) shows that in the RT-550 K the apertures of channels formed by the eight-rings underwent a transient slight opening and regularization associated to the framework relaxation induced by the released hydrogen bonding interactions. This transient phenomenon can be regarded as a "breathing" effect in which the framework initial contraction and distortion is followed by an expansion and regularization, then by a contraction again.

To better evaluate the extent of decoupling and interplay between the water release and the unit cell volume evolution, the differential curves of both trends are compared in Figure 6. A clear correlation exists between the DTG peaks and the maximum contraction steps although the latter appear to be shifted to higher temperature of 60-80 K. To some extent this is expected because the DTG peaks correspond to the middle of the weight loss slope while the maximum contraction occurs at the end of the dehydration step. In addition, we suggest that a little time (temperature) delay exists between the response of the cavansite framework and the water loss due to the kinetic hindrance effect of the dynamic experimental conditions.

In order to gain further insights on the sequence of the water molecules release, the refined occupancies of the O7, O8, and O9 water sites as a function of temperature are plotted in Figure 7 along with the DTG curve. The dehydration of cavansite starts at about 320 K with the onset of water loss from the O9 site. Release from this site seems at stop ~410 K whereupon a little water amount (~0.3 H_2O p.f.u.) is kept up to about 500 K. The water release from the O7 site starts at ~430 K and continuously proceeds up to ~670 K, then this site is sharply emptied at ~730 K. The onset of water loss from the O8 site occurs at ~540 K and this site is fully emptied above 750 K. Thus, based on the water site occupancy refinements, the loss of ~0.7 H_2O p.f.u. at O9 is the responsible for the DTG peak at 366 K. The second DTG peak at 485 K is mostly due to release of about 0.8 H_2O p.f.u. from O7 plus the 0.2 residual water at O9. The third DTG peak at 601 K corresponds to the further release of about 0.5 H_2O p.f.u. from O7 combined with the 0.2 water loss at O8. The fourth DTG peak at 696 K is associated to the loss of the residual 0.7 H_2O p.f.u. from O7. The fifth DTG peak at 751K marking the final water loss in cavansite, corresponds to about 0.8 H_2O p.f.u. from the O8 site. The above water losses appear slightly underestimated compared to those calculated from the thermal curves possibly due to correlation of water occupancies and atomic displacement parameters, as noted before. Nevertheless, the water release sequence appears in good agreement with the findings of Danisi et al. (2012), given the discrepancy on the amount of water released in each step. The most significant difference of our results compared those of Danisi et al. (2012) concerns the positional disorder that these authors described for the O7 and O9 water molecules. According to Danisi et al. (2012), the complete release of H_2O from split O9 and O9a sites in the first dehydration step at 348 K was accompanied by a splitting of O7 H_2O over three positions O7, O7a, and O7b. These three subsites approached the former O9 position during the next dehydration step at 448 K where their sum occupancy decreased to 50%. At 623 K, H_2O was expelled from O8 and the residual H_2O at O7 and O7b moved closer to the former O9 site. Further heating to 673 K was then assumed to remove the residual water from O7 and O7b and cause the cavansite breakdown. We carefully tested the positional disorder model of Danisi et al. (2012) in

our refinement but did not find any evidence for the O9 and O7 split positions. We do not think that this is due to the limited accuracy of our powder diffraction and Rietveld refinements compared to the single crystal data. Instead we suggest that the different time-frame of our data collection compared to that of Danisi et al. (2012) must be taken into account for a more likely explanation. In our experiment each XRD snapshot collects simultaneously the whole reciprocal lattice in 5 minutes. Each single crystal data collection of Danisi et al. (2012) typically took 480 minutes with 'at least 30 min' annealing time before data collection. We experienced, in our own HT single crystal work, that a too short equilibration time would lead the crystal structure of a zeolite heated *in situ* to be still changing during a relatively long measurement. Since different portions of the Ewald sphere are typically registered in sequence by CCD images, this would result in an integration of different crystal structure arrangements, changing over the 480 minutes, into a single snapshot. In other words we speculate that the positional disorder found by Danisi et al. (2012) at a given temperature (time) step could actually reflect the overlap of different arrangements of water positions changing in time. As a matter of fact, in their *ex situ* single crystal work Rinaldi et al. (1975) did not find any evidence for splitting of O7 and W1, the latter being the only water molecule left at 493 K in their experimental conditions which they refined with anisotropic displacement parameters. For another possible explanation we note that the much slower diffusion in large (i.e. tenths of millimeter size) single crystals compared to submicrometer size powders makes the former very prone to formation of domains with different structural arrangements and cracks due to tensions between domains. The single crystal of Danisi et al. (2012) was broken after the first dehydration step very likely due to internal strain. The occurrence of 10% vanadium pyramids with flipped orientation found *ex situ* by Rinaldi et al. (1975), but not observed *in situ* by Danisi et al. (2012), is another sign of possible formation of domains that might be interpreted as disorder. It seems therefore reasonable that, unlike Danisi et al. (2012), we did not observe the split positions for water molecules due to our very different experimental conditions (fast and simultaneous data collection, submicron crystals). Instead, we cannot rule out that the ~0.2 H_2O

p.f.u. hosted in the O9 site at ~460 K (see Figure 7) might have originated from O7 whose water loss had started in the meantime. It is to be noted that the sum of occupancy fractions of O7 and O9 at this temperature is close to 1.0 and is consistent with their short intersite distance (1.87 Å). A similar consideration applies to the partial refilling of ~0.2 H_2O the O8 site at ~720 K while the occupancy of O7 drops. The occupancy of O7 and O8 at ~720 K is acceptable within the error considering the very short distances O7-O8 (1.21 Å) and O7-O7 (1.00 Å) which prevent these water sites to be occupied simultaneously.

The evolution of the crystal structure is sketched in Figure 8 for four reference temperature steps (298 K, 433 K, 542 K, 783 K). Concerning in particular the change in the coordination shell of Ca, our results fully support the findings of Danisi et al. (2012): the H_2O expulsion starting at O9, which has the longest distance from Ca at RT, is accompanied by a further increases of the Ca-O9 bond distance from 2.869 Å (at 298 K) to 3.064 Å (at 380 K). With the O7 site becoming vacant at ~720 K, Ca ions approached the framework oxygens and consequently the mean Ca-O distance decreased to 2.294 Å. When the last dehydration step occurred (DTG peak at 751 K) and the residual H_2O content was completely expelled at T>783 K from the O8 site (Figure 9), the latter possibly being a subsite of former O7 in agreement with Danisi et al. (2012), the Ca ions attacked the framework oxygens. This displacement of the Ca ions induced a sharp increase in the counter-rotation around the O5 oxygens acting as hinges of the four-rings in the plane of the cavansite silicate layers. This counter-rotation was thus responsible for an dramatic squashing of the eight-ring channels delimited by the O5 oxygens (see Figure 8), the Si(1)-O5-Si(2) angle equal to 125° at 810 K, leading to a minimum free diameter O5-O5 as low as 1.5 Å (calculated assuming an effective radius of 1.35 Å for oxygen) at 810 K. It is conceivable that such an extreme collapse of the channels, hampering the diffusion of the last H_2O molecules leaving the zeolite, caused much instability of the cavansite structure leading to its breakdown. In our refinement at 810 K, just before the cavansite breakdown, we did not find any indication for a possible polymorphic phase transition to pentagonite at HT as speculated by Evans (1973) and Ishida et al. (2009).

4. Conclusions

Inspired by the accurate single crystal *in situ* HT work of Danisi et al. (2012), performed under static near-equilibrium conditions, we extended the structural investigation upon heating of cavansite to the out-of-equilibrium dynamic conditions reproduced by the *in situ* time resolved powder diffraction experiment using synchrotron radiation. The general picture of cavansite dehydration, including the sequence of release of water molecules and the associated change in coordination of Ca cations leading to the final structural breakdown, that we found in present work is in fairly good agreement with that previously reported by Danisi et al. (2012). Owing to the closer experimental conditions between thermogravimetric analyses and time-resolved XRD, we better explained the nearly continuous nature of water loss observed in the TG curves by Ishida et al. (2009) and ours and the occurrence of five DTG peaks. We provided clear-cut confirmation that there is no sign for the polymorphic phase transition at HT from cavansite to pentagonite as envisaged by Evans (1973) and Ishida et al. (2009).

As the most significant and unique result of our study compared to what previously done, we were able to monitor one important transient phenomenon of the type that can only be detected under dynamic out-of-equilibrium conditions. This phenomenon is the cell volume expanding framework relaxation in the initial heating stages which resulted from breakdown of the firmly cross-linked hydrogen bonding system nicely described at RT by Danisi et al. (2012). This phenomenon brought about a short-lived "breathing" of the cavansite framework which is a dynamic effect typical of many zeolite-like flexible network structures. This kind of effects are regarded with much interest because they can be exploited in applications, such as gas separation, for fine tuning of zeolite channel apertures or for engineering of kinetically hindered mechanisms such as the "trap door" effect (Reisner et al. 2000). Figure 5 clearly shows that under the dynamic heating conditions of a possible industrial application cavansite exhibits a clear cross-over temperature (~550 K) below which the its framework undergoes "breathing" with three recognizable pulses. Above 550 K the

transient cell-expanding effect has ended and the framework proceeds to an progressive squashing of eight-ring channels assisted by the counter-rotations around the 4MR-O5-4MR hinges. A similar behaviour was also observed in cavansite under high-pressure conditions (Danisi et al., 2015) when the T-O-T angles antirotate while the V-O-T angles corotate when the volume decrease. We found that the extreme collapse of the elliptical apertures leaving just 1.5 Å a minimum free diameter, along with the reduced Ca coordination in agreement with Danisi et al. (2012), leads to the amorphization of cavansite.

5. Acknowledgements

References

Ardit, M., Martucci, A., Cruciani, G. (2015): Monoclinic–Orthorhombic Phase Transition in ZSM-5 Zeolite: Spontaneous Strain Variation and Thermodynamic Properties. J. Phys. Chem. C, **119**, 7351-7359.

Cruciani, G. and Gualtieri, A.F. (1999): Dehydration dynamics of analcime by in situ synchrotron powder diffraction, Am. Miner., **84**, 112–119.

Danisi, R.M., Armbruster, T., and Lazic, B. (2012): In situ dehydration behavior of zeolite-like cavansite: a single crystal X ray study. Am. Mineral. , **97**, 1874–1880.

Danisi, R.M., Armbruster, T., Arletti, R., Gatta, D., Vezzalini, G., Quartieri, S., Dmitriev, V., (2015): Elastic behavior and pressure-induced structural modification of the microporous $Ca(VO)Si_4O_{10} \cdot 4H_2O$ dimorphs cavansite and pentagonite. Micropor. Mesopor. Mat., **204**, 257–268.

Evans, H.T. Jr. (1973) The crystal structures of cavansite and pentagonite. Am. Mineral., **58**, 412–424.

Felsche, J., and Luger, S. (1986): Structural Collapse or Expansion of the Hydro-Sodalite Series $Na_8[AlSiO_4]_6(OH)_2 \cdot nH_2O$ and $Na_6[AlSiO_4]_6 \cdot nH_2O$ upon Dehydratation. Ber. Bunsenges. Phys. Chem., **90,** 731–736**.**

Hughes, J.M., Derr, R.S., Cureton, F., Campana, C.F., and Druschel, G. (2011): The crystal structure of cavansite: location of the H_2O water molecules and hydrogen atoms in $Ca(VO)(Si_4O_{10}) \cdot 4H_2O$. Can. Mineral., **49**, 1267–1272.

Ishida, N., Kimata, M., Nishida, N., Hatta, T., Shimizu, M., and Akasaka, T. (2009): Polymorphic relation between cavansite and pentagonite; genetic implications of oxonium ion in cavansite. J. Miner. Petrol. Sci., **104**, 241-252.

Kothavala, R. Z. (1991): The Wagholi Cavansite locality near Poona, India. Mineral. Rec , **22**, 415-420.

Larson, A.C. Von Dreele R.B. (2000): General Structure Analysis System (GSAS), Los Alamos National Laboratory Report LAUR, 86–748.

Leardini, L., Martucci, A., Cruciani, G. (2012): The unusual thermal expansion of pure silica sodalite probed by in situ time-resolved synchrotron powder diffraction. Micropor. Mesopor. Mat., **151,** 163–171.

Makki, M.F. (2005): Collecting cavansite in the Wagholi Quarry complex, Pune, Maharashtra, India. Mineral. Rec , **36**, 507-512.

Martucci, A., Rodeghero, R. , Pasti, L., Bosi, V. and Cruciani, G. (2015): Adsorption of 1,2-dichloroethane on ZSM-5 and desorption dynamics by in situ synchrotron powder X-ray diffraction, Micropor. Mesopor. Mat., 215, 175–182.

Meneghini, C., G. Artioli, A. Balerna, A. F. Gualtieri, P. Norby, and S. Mobilio (2001): Multi purpose imaging plate camera for in-situ powdern XRD at the GILDA beamlinen. J. Synchrotron Rad., **8**, 1162–1166.

Milazzo, E., Artioli, G., Gualtieri, A., and Hanson, J.C. (1998): The dehydration process in gismondine: An in situ Synchrotron XRPD study. Proocedings IV Convegno Nazionale Scienza e Tecnologia delle Zeoliti, 160-165.

Pietrzyk, P., Sojka, Z., Dzwigaj, S. and Che, M. (2007) Generation, Identification, and Reactivity of Paramagnetic VO Centers in Zeolite BEA for Model Studies of Processes Involving Spin Pairing, Electron Transfer, and Oxygen Transfer. J. Am. Chem. Soc., **129**, 14174-14175.

Prasad, P.S.R. and Prasad, S.K. (2007): Dehydration behavior of natural cavansite: an in-situ FTIR and Raman spectroscopic study. Mater. Chem. Phys., **105**, 395-400.

Reisner, B.A, Lee, Y, Hanson, J.C, Jones, G.A, Parise, J.B, Corbin, D.R, Toby, B.H, Freitag, A., Larese, J.Z, Kahlenberg, V. (2000) Understanding negative thermal expansion and 'trap door' cation relocations in zeolite rho. Chem. Commun., **22**, 2221–2222.

Rinaldi, R., Pluth, J.J., and Smith, J.V. (1975): Crystal structure of cavansite dehydrated at 220°C. Acta Cryst., **B31**, 1598–1602.

Seryotkin, Y.V., Joswig, W. , Bakakin, V.V., Belitsky, I.A., Fursenko, B.A. (2003): High-temperature crystal structure of wairakite, Eur. J. Miner., **15**, 475–484.

Solov'ev, M.V., Rastsvetaeva, R.K., and Pushcharovskii, D.Y. (1993): Refined crystal structure of kavansite. Crystallogr. Rep., **38**, 274–275.

Toby, B.H. (2001): EXPGUI, a graphical user interface for GSAS, J. Appl. Crystallogr., 210–213.

Wang, X., Lumei, L., Jacobson, A.J. (2002): Open-framework and microporous vanadium silicates. J. Am. Chem. Soc., **124**, 7812-7820.

Figure Captions.

Figure 1. TG and DTG curves of cavansite from Poona (this work, continuous lines) compared to TG curve digitalized from Figure 1a of Ishida et al. (2009) and corresponding DTG curve (broken line).

Figure 2. Selected powder patterns of cavansite as a function of temperature.

Figure 3. Change of the water content as obtained from Rietveld structure refinements (gray broken line) and as calculated from the thermogravimetric analysis (grey dotted line) compared to the evolution of the cavansite cell volume of cavansite (continous line) as a function of temperature.

Figure 4. Temperature dependence of the unit-cell parameters and volume as normalized values, $a(T)/a_0$, $b(T)/b_0$, $c(T)/c_0$, and $V(T)/V_0$ with a_0, b_0, c_0, and V_0 being the references refined at 298K. Error bars are smaller than symbols.

Figure 5. Variation of the O5-O5 distances defining the short and long axes of the elliptically shaped eight-membered tetrahedral rings.

Figure 6. Comparison of temperature development of DTG (continous line) and differential unit cell volume curves (broken line).

Figure 7. Evolution as a function of temperature of the site occupancy fraction of individual water molecules (O7=white square, O8=grey diamond, O9=black circle) compared to the DTG curve (broken line).

Figure 8. Framework of cavansite at 298 K (a), 433 K (b), 542 K and 783 K, respectively.

Figure 9. Comparison of Ca coordination environment at 298K and 783K.
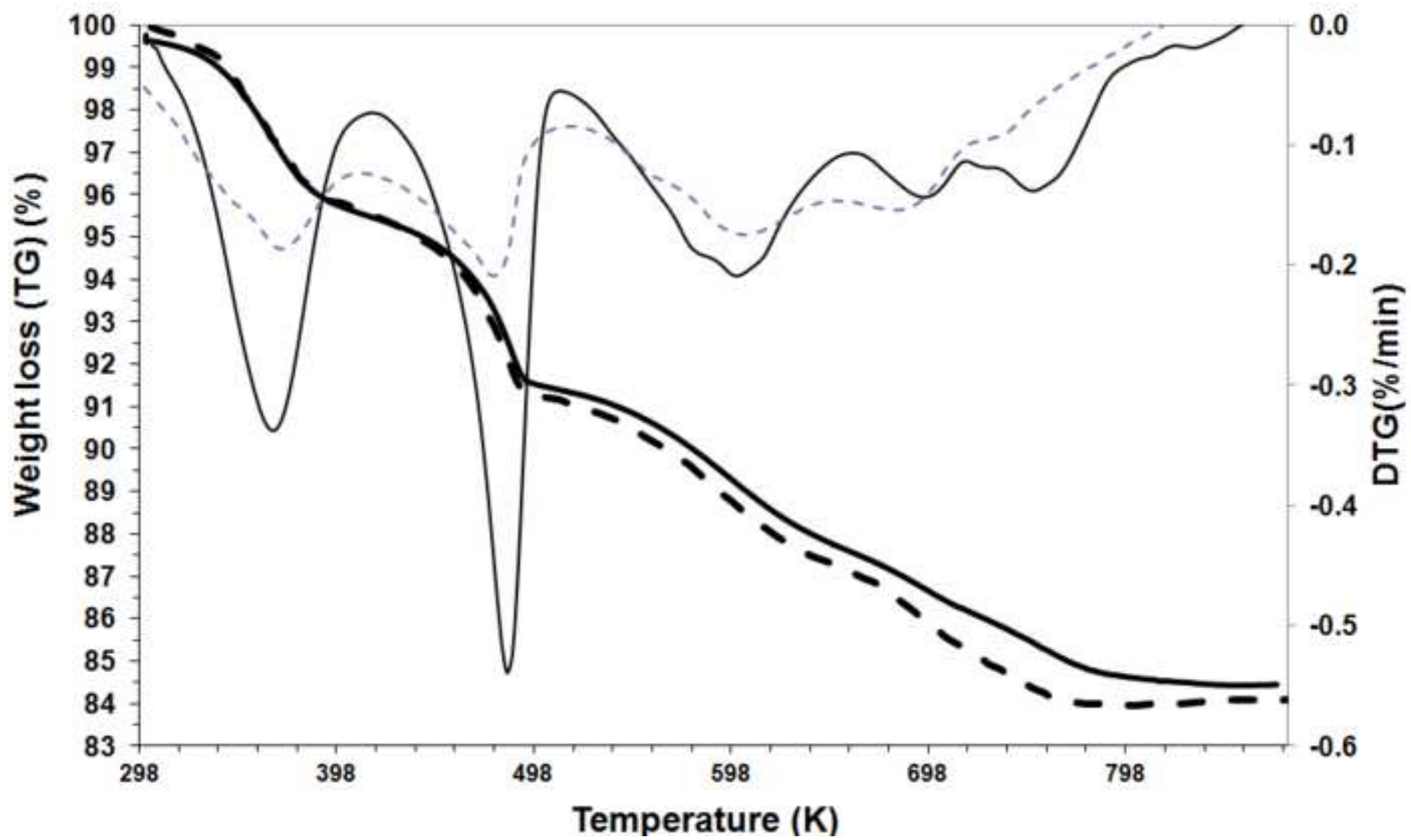
Figure 1
Click here to download Figure: Figure 1.tif

Figure 1

Figure 2

Figure 3
Click here to download Figure: Figure 3.tif

Figure 3

Figure 4

Figure 5
Click here to download Figure: Figure 5.tif

Figure 5

Figure 6

Figure 7
Click here to download Figure: Figure 7.tif
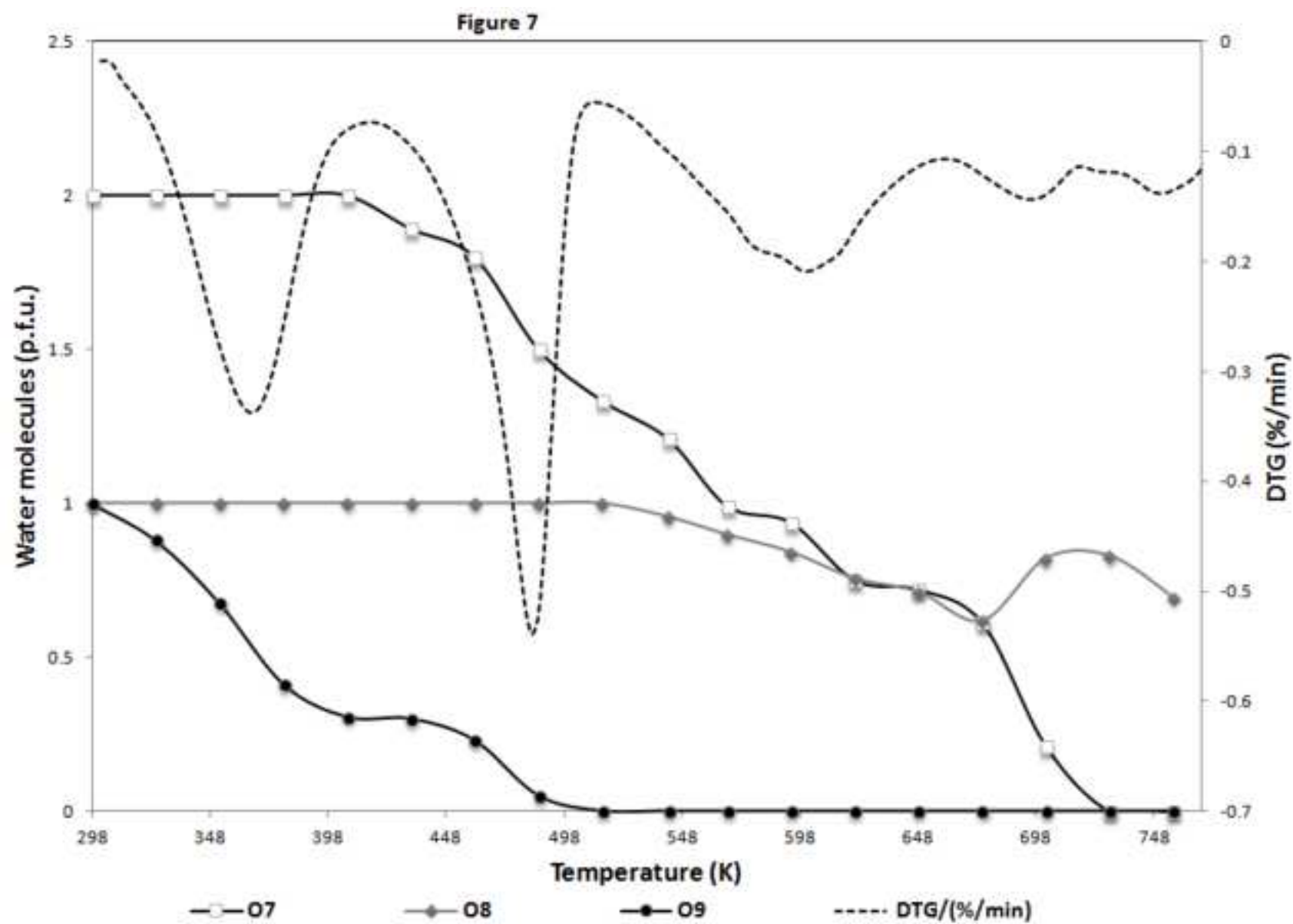
Figure 7
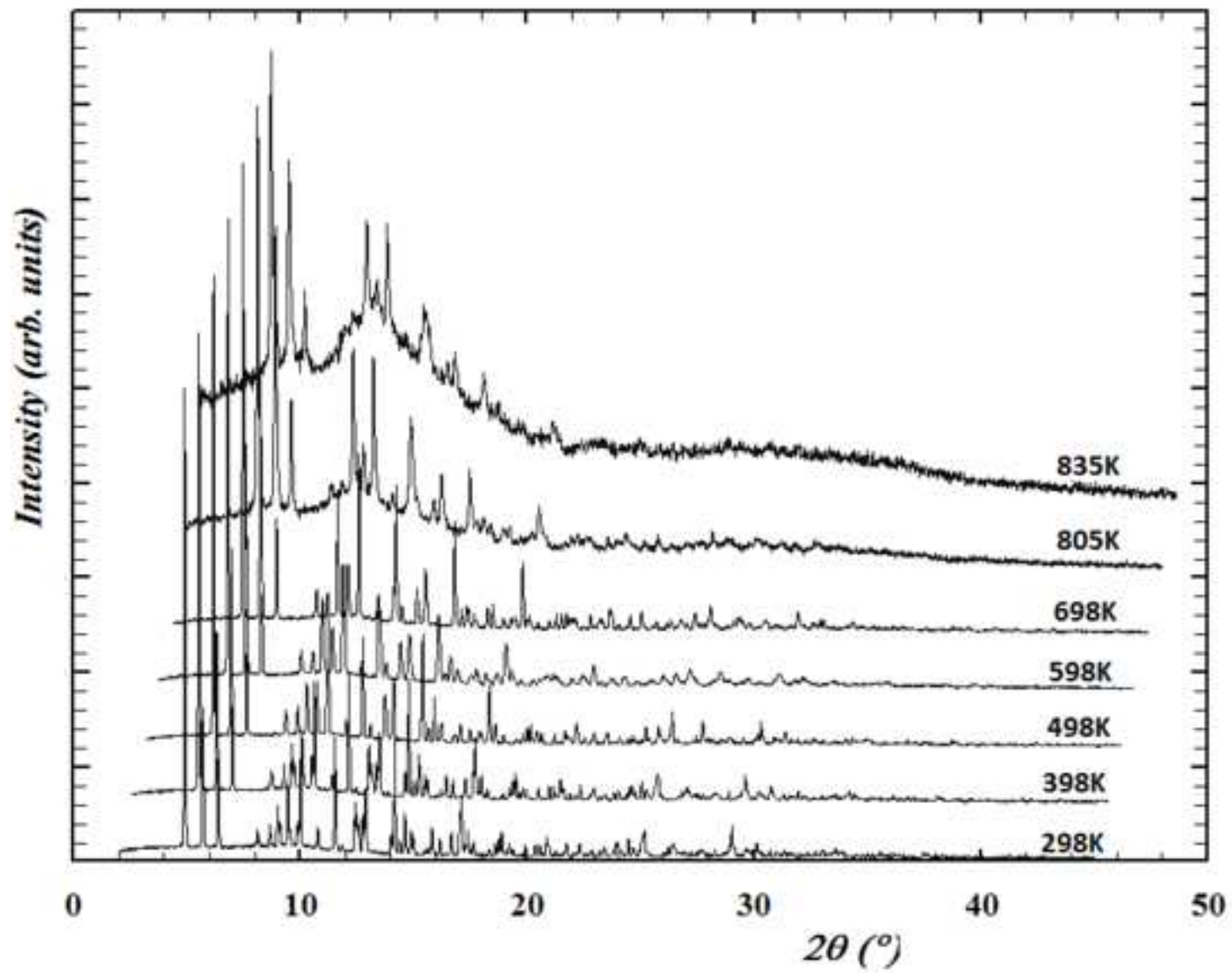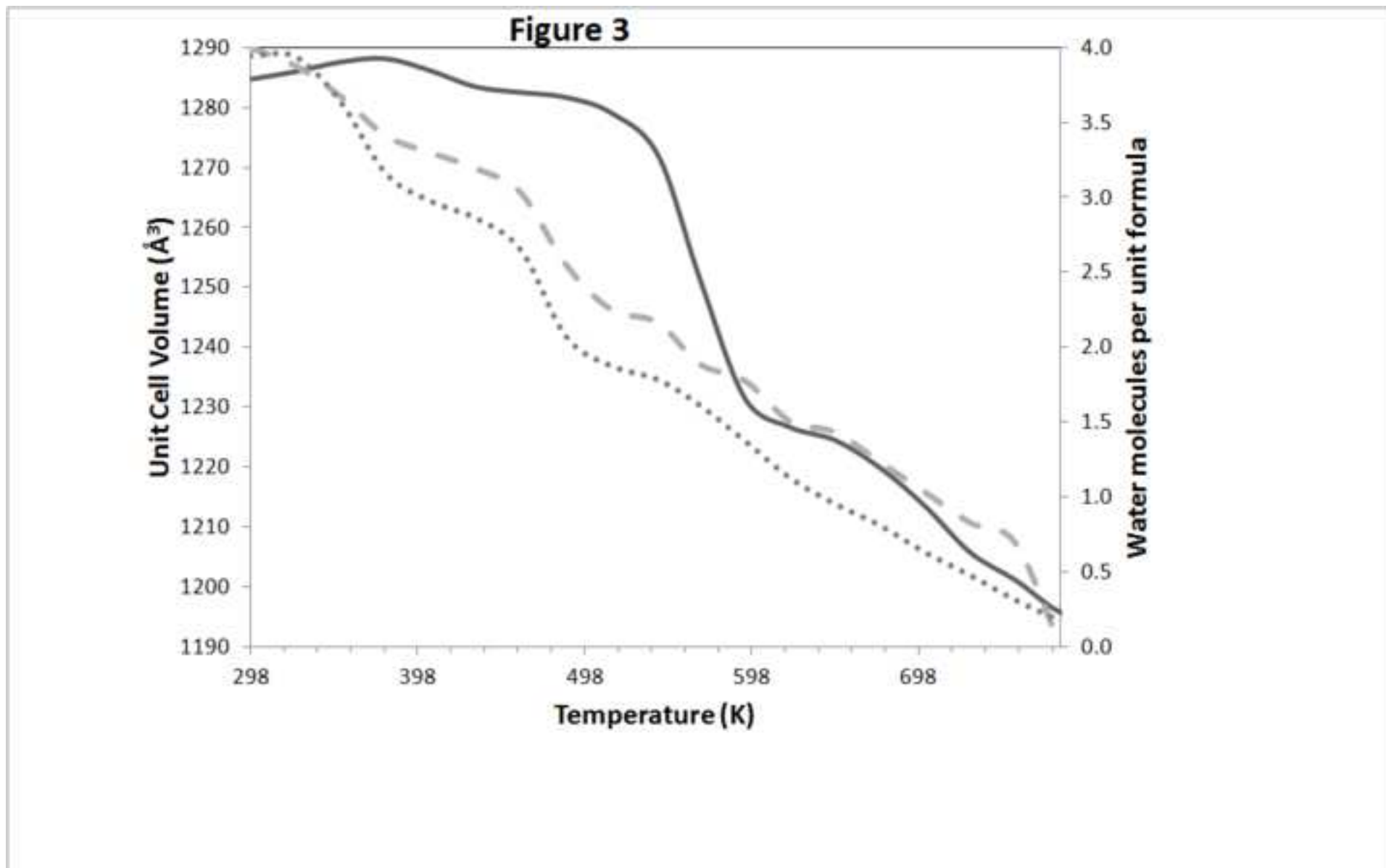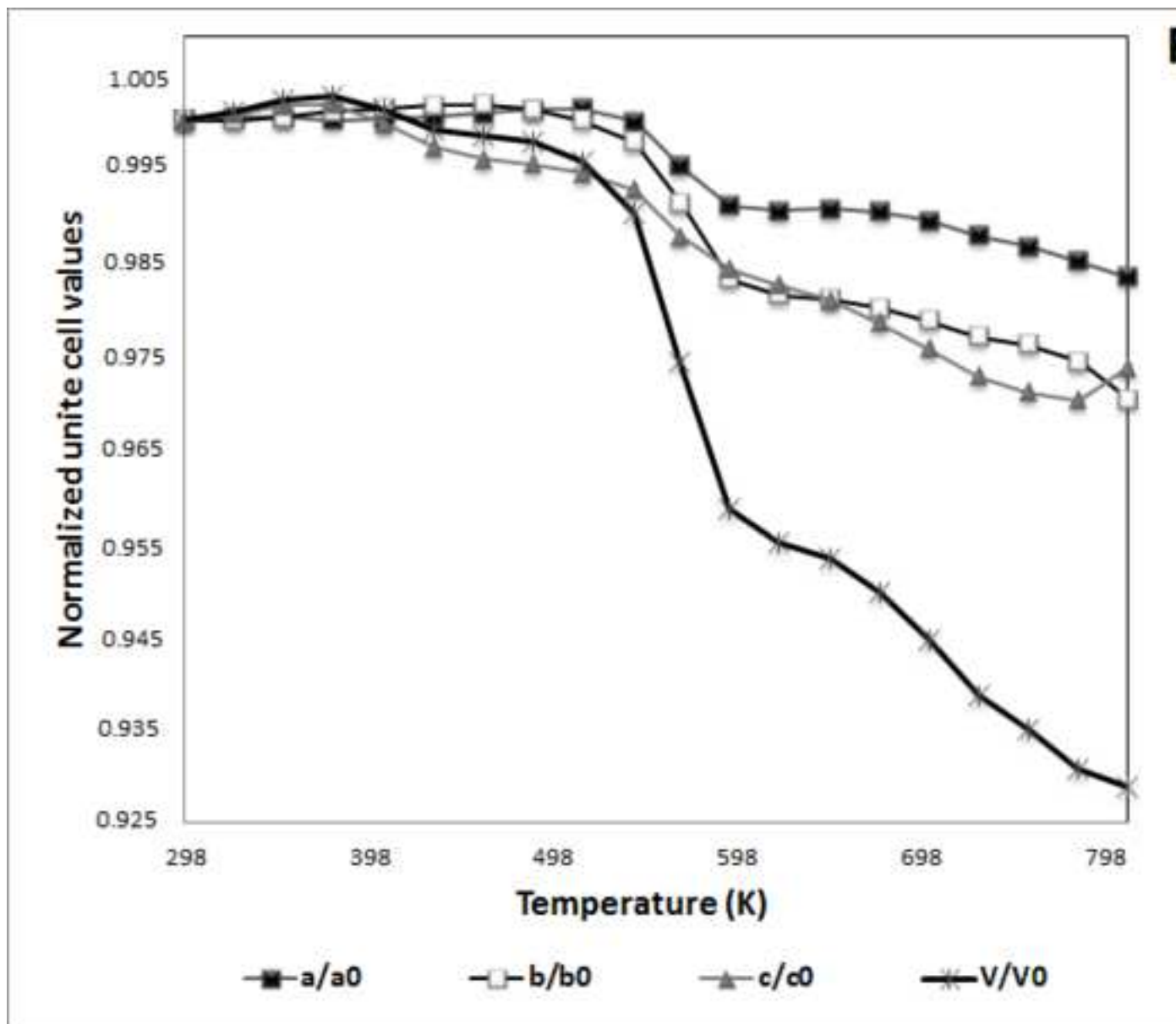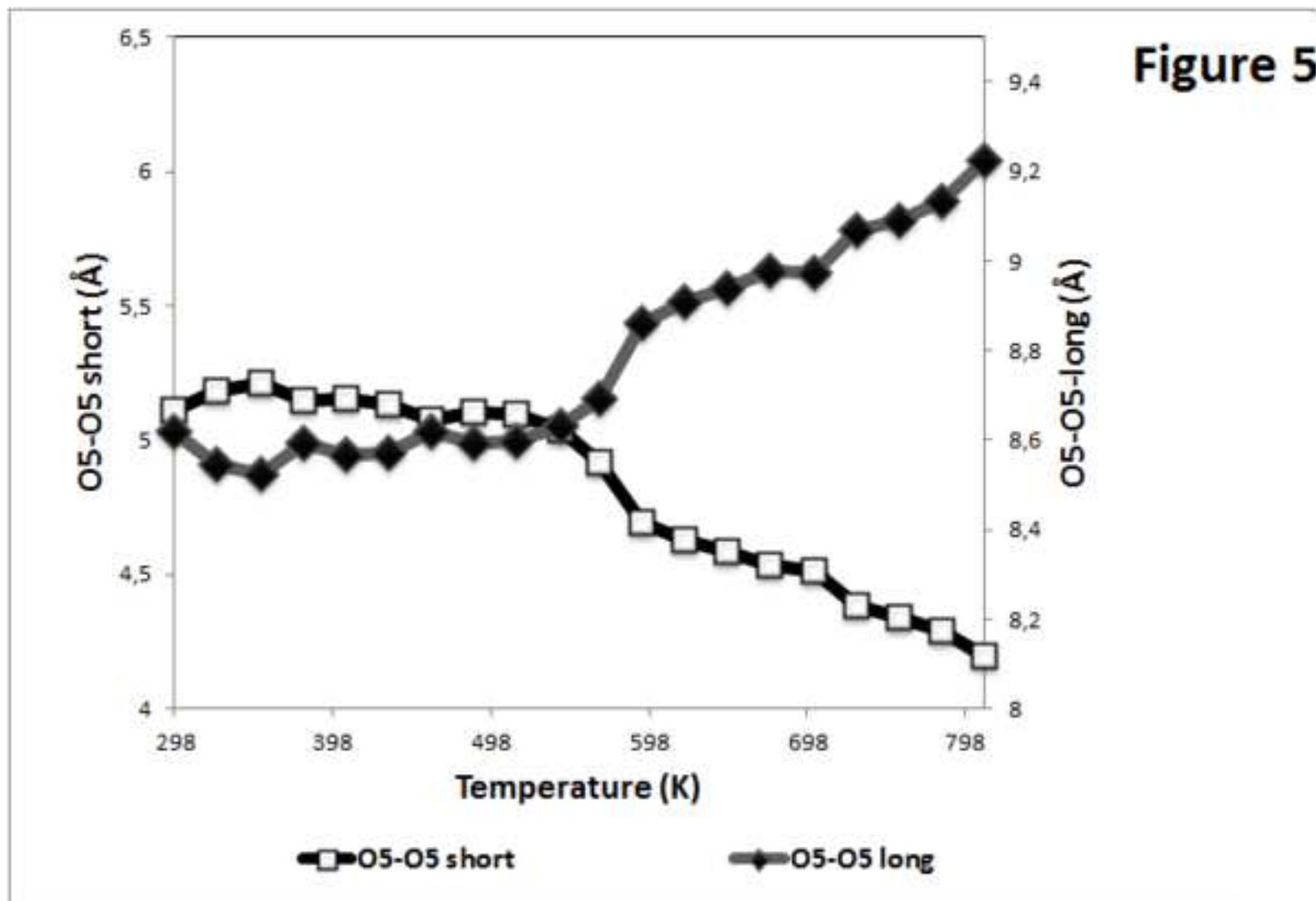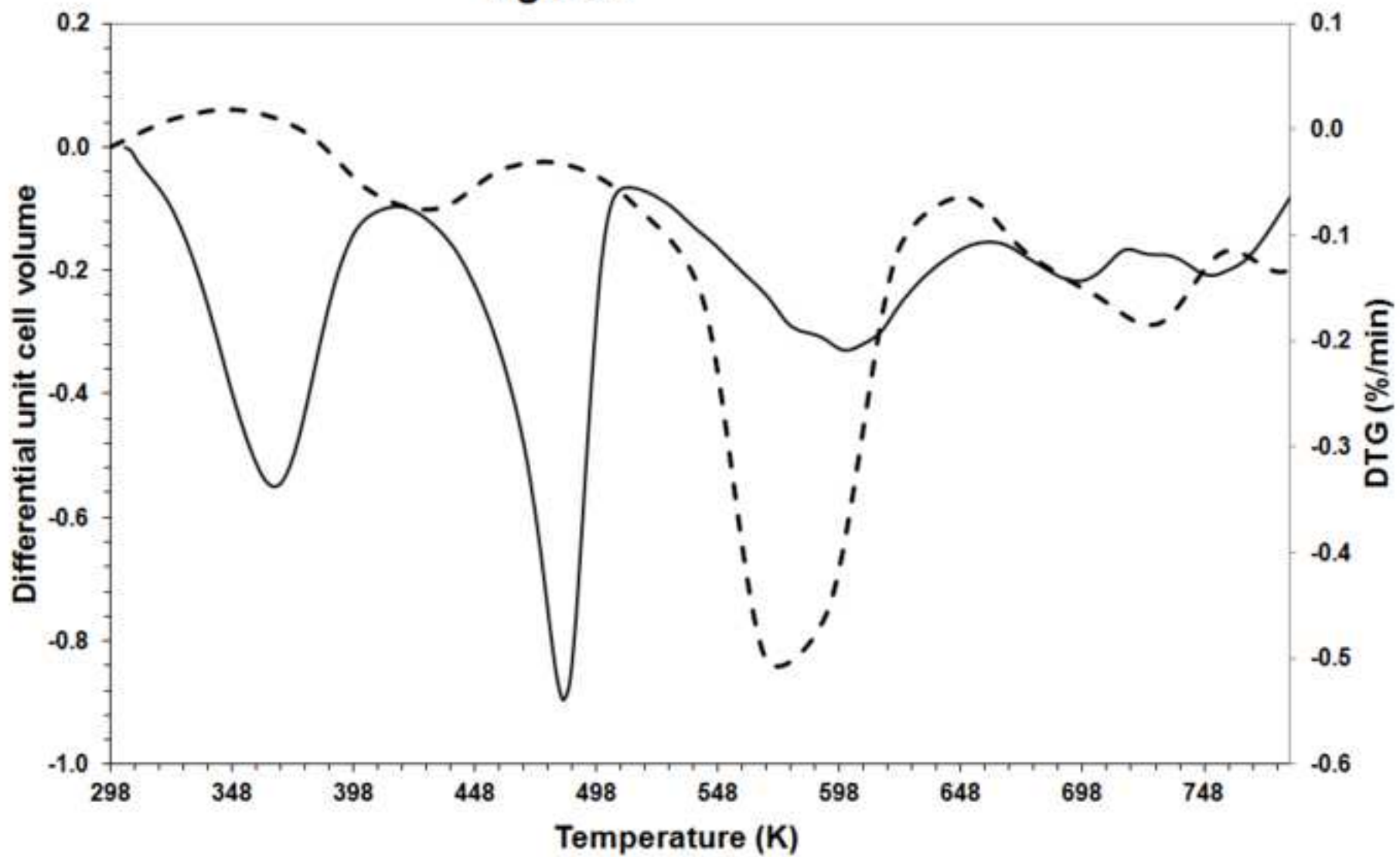
Figure 8
Click here to download Figure: Figure 8.tif

Figure 8

Figure 9
Click here to download Figure: Figure 9.tif
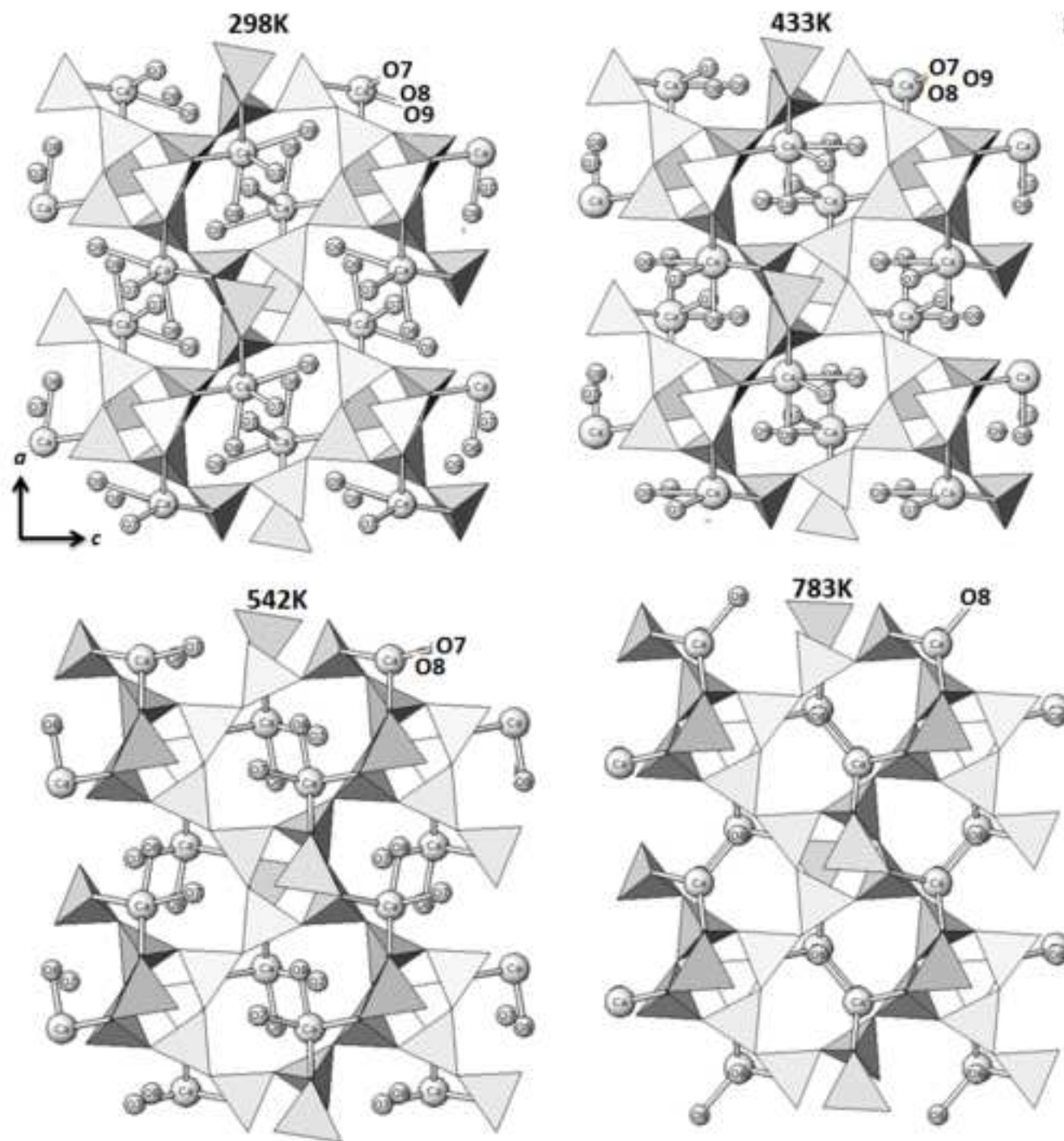
Figure 9
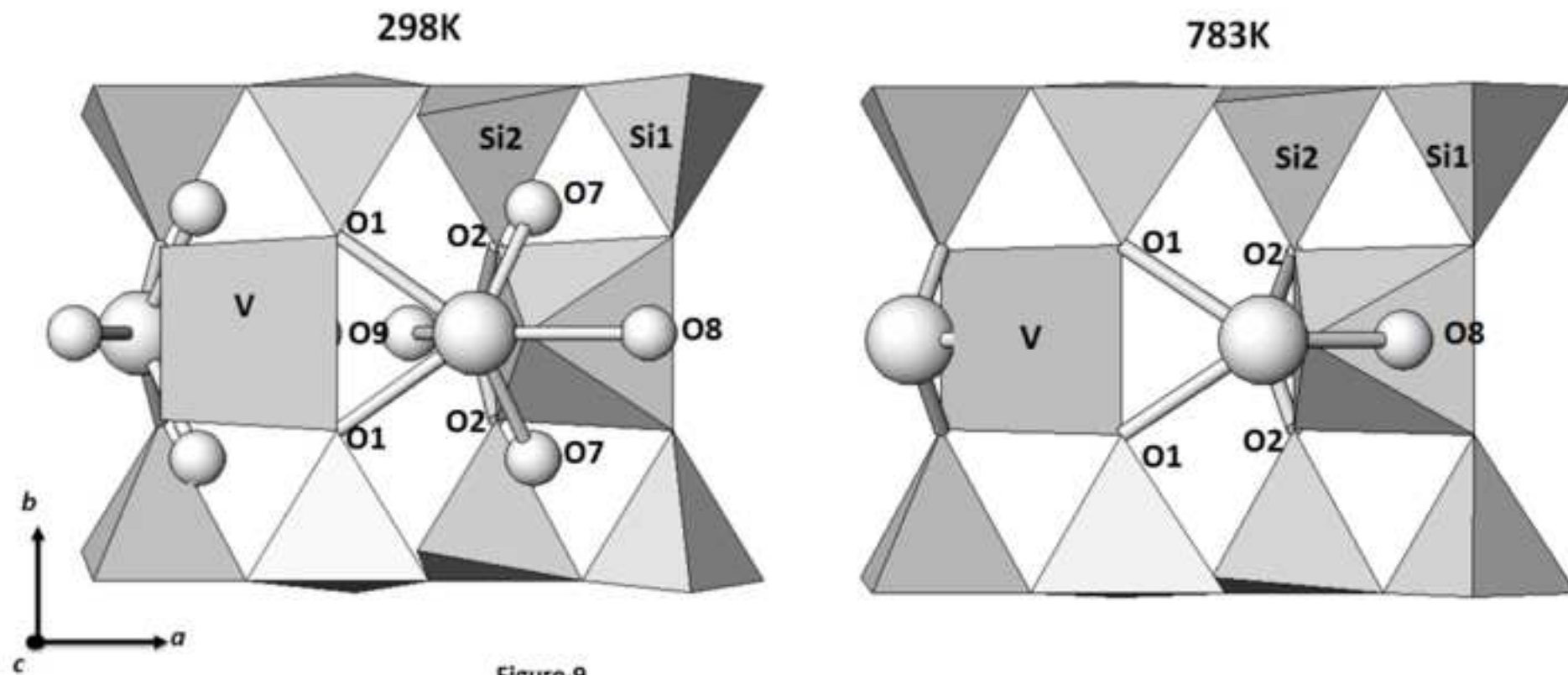
Table 1

Table 1. Lattice parameters and refinement details for Cavansite at 298, 433, 542 and 783 K.

	298 K	433 K	542 K	783 K
Space group	*Pnma*	*Pnma*	*Pnma*	*Pnma*
a (Å)	9.6197(3)	9.6213(3)	9.6191(4)	9.4826(15)
b (Å)	13.6526(4)	13.6794(4)	13.6202(5)	13.3074(20)
c (Å)	9.7819(3)	9.7790(4)	9.7091(4)	9.4864(25)
$\alpha=\gamma=90°$	90	90	90	90
V (Å^3)	1284.70(7)	1286.09(9)	1272.02(9)	1197.07(46)
Wavelength of incident radiation (Å)	0.68765(1)	0.68765(1)	0.68765(1)	0.68765(1)
Refined pattern 2θ range (°)	2.3-44.6	2.3-44.6	2.3-44.6	2.3-44.6
R_{wp} (%)	9.13	8.79	8.34	5.96
R_p (%)	7.2	7.00	6.71	4.52
R_F^2 (%)	13.2	13.7	11.7	8.1
N_o of contributing reflections	2835	2836	2835	2835
N_{obs}	1005	988	1009	1028
N_{var}	66	66	61	56

Supplementary Information

Continuous dehydration of cavansite under dynamic conditions by *in situ* synchrotron powder diffraction

A. Martucci, E. Rodeghero and G. Cruciani

Corresponding author:

Annalisa Martucci,

Università degli Studi di Ferrara

Department of Physics and Earth Sciences,

I-44100 - Ferrara

Tel: +39-(0)532-974730

Fax: +39 (0)532-210161

Supplementary information layout:

Table 1 SI. Atomic fractional coordinates, fraction and Uiso of cavansite at 298 K.

Table 2 SI. Atomic fractional coordinates, fraction and Uiso of cavansite at 433 K.

Table 3 SI. Atomic fractional coordinates, fraction and Uiso of cavansite at 542 K.

Table 4 SI. Atomic fractional coordinates, fraction and Uiso of cavansite at 783 K.

CIF FILE of cavansite at 298 K.

CIF FILE of cavansite at 433 K.

CIF FILE of cavansite at 542 K.

CIF FILE of cavansite at 783 K.

Table 1 SI. Atomic fractional coordinates, fraction and Uiso of cavansite at 298 K.

	x/a	y/b	z/c	Ui/Ue*100	Fractn
V	0.0268(1)	0.25	0.0973(1)	1.79(18)	1.00
Ca	-0.3823(6)	0.75	-0.0836(6)	1.94(21)	1.00
Si1	-0.1828(6)	0.5331(4)	-0.0946(6)	1.60(13)	1.00
Si2	-0.1094(6)	0.4527(5)	0.1860(6)	1.60(13)	1.00
O1	-0.1764(12)	0.6476(7)	-0.0883(12)	1.30(17)	1.00
O2	-0.0864(13)	0.3415(8)	0.2070(11)	1.30(17)	1.00
O3	-0.2042(12)	0.4780(9)	0.0507(11)	1.30(17)	1.00
O4	-0.0414(13)	0.4902(9)	-0.1680(11)	1.30(17)	1.00
O5	-0.3130(13)	0.4900(8)	-0.1851(11)	1.30(17)	1.00
O6	-0.0411(16)	0.250000	-0.0545(15)	1.30(17)	1.00
O7	-0.4691(12)	0.8813(8)	0.0544(11)	6.66(40)	1.00
O8	-0.6414(17)	0.750000	-0.1195(18)	6.66(40)	1.00
O9	-0.2861(21)	0.750000	0.1940(20)	6.66(40)	1.00

Table 2 SI. Atomic fractional coordinates, fraction and Uiso of cavansite at 433 K

	x/a	y/b	z/c	Ui/Ue*100	Fractn
V	0.0271(5)	0.25	0.0923(6)	1.99(18)	1.00
Ca	-0.3808(6)	0.75	-0.0893(7)	1.89(20)	1.00
Si1	-0.1843(6)	0.5325(4)	-0.0946(6)	1.54(12)	1.00
Si2	-0.1105(6)	0.4547(4)	0.1866(6)	1.54(12)	1.00
O1	-0.1754(7)	0.6495(4)	-0.0871(13)	1.25(16)	1.00
O2	-0.0873(11)	0.3393(4)	0.2051(9)	1.44(16)	1.00
O3	-0.1992(9)	0.4809(8)	0.0523(7)	1.49(16)	1.00
O4	-0.0406(7)	0.4978(6)	-0.1631(11)	1.21(16)	1.00
O5	-0.3113(9)	0.4942(6)	-0.1870(9)	1.13(16)	1.00
O6	-0.0434(15)	0.250000	-0.0547(9)	2.69(16)	1.00
O7	-0.4575(13)	0.8713(9)	0.0689(12)	6.68(10)	1.00
O8	-0.6351(19)	0.750000	-0.0994(21)	7.82(10)	1.00
O9	-0.3434(59)	0.750000	0.1874(52)	12.99(28)	0.31(1)

Table 3 SI. Atomic fractional coordinates, fraction and Uiso of cavansite at 542 K

	x/a	y/b	z/c	Ui/Ue*100	Fractn
V	0.0237(5)	0.25	0.0918(6)	2.16(19)	1.00
Ca	-0.3783(7)	0.75	-0.0876(8)	2.65(23)	1.00
Si1	-0.1890(8)	0.5331(4)	-0.0901(7)	2.34(13)	1.00
Si2	-0.1055(7)	0.4535(5)	0.1898(7)	2.30(13)	1.00
O1	-0.1739(7)	0.6504(4)	-0.0923(15)	2.43(16)	1.00
O2	-0.0845(13)	0.3380(5)	0.2138(10)	2.62(16)	1.00
O3	-0.1987(11)	0.4808(10)	0.0580(8)	2.67(16)	1.00
O4	-0.0454(8)	0.4999(7)	-0.1609(12)	2.39(16)	1.00
O5	-0.3153(11)	0.4945(7)	-0.1838(10)	2.31(16)	1.00
O6	-0.0405(18)	0.250000	-0.0591(10)	3.87(16)	1.00
O7	-0.4308(26)	0.8459(20)	0.1186(28)	11.56(18)	0.61(2)
O8	-0.6146(29)	0.750000	-0.0486(26)	12.51(14)	1.00

Table 4 SI. Atomic fractional coordinates, fraction and Uiso of cavansite at 783 K

	x/a	y/b	z/c	Ui/Ue*100	Fractn
V	0.0270(15)	0.25	0.0834(17)	2.5(6)	1.00
Ca	-0.3872(28)	0.75	-0.0852(27)	5.5(9)	1.00
Si1	-0.1884(24)	0.5344(15)	-0.0826(24)	4.0(6)	1.00
Si2	-0.0941(20)	0.4593(13)	0.2110(29)	3.9(6)	1.00
O1	-0.1853(20)	0.6540(15)	-0.0623(37)	6.2(7)	1.00
O2	-0.0692(45)	0.3403(14)	0.2187(26)	6.4(7)	1.00
O3	-0.1848(45)	0.4899(33)	0.0747(24)	6.4(7)	1.00
O4	-0.0576(22)	0.4941(18)	-0.1740(44)	6.1(7)	1.00
O5	-0.3322(30)	0.4939(21)	-0.1515(28)	6.1(7)	1.00
O6	-0.0536(57)	0.250000	-0.0635(28)	7.6(7)	1.00
O8	-0.5855(111)	0.750000	0.0811(114)	16.15(18)	0.69(5)

CIF FILE of cavansite at 298 K.

```
# from I:/BACKUP~1/VOLUME~1/ARD9E5~1/cava298K
_audit_creation_date            2015-03-30T10:32:14
_symmetry_space_group_name_H-M     'P nma'
_cell_length_a     9.61974(29)
_cell_length_b     13.6526(4)
_cell_length_c     9.78188(34)
_cell_angle_alpha     90.0000
_cell_angle_beta     90.0000
_cell_angle_gamma      90.0000
loop_
 _atom_site_label
 _atom_site_type_symbol
 _atom_site_fract_x
 _atom_site_fract_y
 _atom_site_fract_z
 _atom_site_B_iso_or_equiv
 _atom_site_occupancy
V V 0.02684(5) 0.25000 0.09729(6) 1.79(18) 1.00000
Ca CA -0.3823(6) 0.75000 -0.0836(6) 1.94(21) 1.00000
Si1 SI -0.1828(6) 0.5331(4) -0.0946(6) 1.60(13) 1.00000
Si2 SI -0.1094(6) 0.4527(5) 0.1860(6) 1.60(13) 1.00000
O1 O -0.1764(12) 0.6476(7) -0.0883(12) 1.30(17) 1.00000
O2 O -0.0864(13) 0.3415(8) 0.2070(11) 1.30(17) 1.00000
O3 O -0.2042(12) 0.4780(9) 0.0507(11) 1.30(17) 1.00000
O4 O -0.0414(13) 0.4902(9) -0.1680(11) 1.30(17) 1.00000
O5 O -0.3130(13) 0.4900(8) -0.1851(11) 1.30(17) 1.00000
O6 O -0.0411(16) 0.25000 -0.0545(15) 1.30(17) 1.00000
O7 O -0.4691(12) 0.8813(8) 0.0544(11) 6.66(40) 1.00000
O8 O -0.6414(17) 0.75000 -0.1195(18) 6.66(40) 1.00000
O9 O -0.2861(21) 0.75000 0.1940(20) 6.66(40) 1.00000
```

CIF FILE of cavansite at 433 K.

```
# from D:/armbruster/cava130/CAVANSITE433K
_audit_creation_date            2015-06-29T15:45:28
_symmetry_space_group_name_H-M     'P nma'
_cell_length_a     9.62127(32)
_cell_length_b     13.6694(4)
_cell_length_c     9.7790(4)
_cell_angle_alpha     90.0000
_cell_angle_beta     90.0000
_cell_angle_gamma     90.0000
loop_
 _atom_site_label
 _atom_site_type_symbol
 _atom_site_fract_x
 _atom_site_fract_y
 _atom_site_fract_z
 _atom_site_B_iso_or_equiv
 _atom_site_occupancy
V V 0.0271(5) 0.25000 0.0923(6) 1.99(18) 1.00000
Ca CA -0.3808(6) 0.75000 -0.0893(7) 1.89(20) 1.00000
Si1 SI -0.1843(6) 0.5325(4) -0.0946(6) 1.54(12) 1.00000
Si2 SI -0.1105(6) 0.4547(4) 0.1866(6) 1.51(12) 1.00000
O1 O -0.1754(7) 0.6495(4) -0.0871(13) 1.25(16) 1.00000
O2 O -0.0873(11) 0.3393(4) 0.2051(9) 1.44(16) 1.00000
O3 O -0.1992(9) 0.4809(8) 0.0523(7) 1.49(16) 1.00000
O4 O -0.0406(7) 0.4978(6) -0.1631(11) 1.21(16) 1.00000
O5 O -0.3113(9) 0.4942(6) -0.1870(9) 1.21(13) 1.00000
O6 O -0.0434(15) 0.25000 -0.0547(9) 2.69(16) 1.00000
O7 O -0.4575(13) 0.8713(9) 0.0689(12) 6.68(10) 1.00000
O8 O -0.6351(19) 0.75000 -0.0994(21) 7.82(10) 1.00000
O9 O -0.3434(59) 0.75000 0.1874(52) 12.99(28) 0.305(5)
```

CIF FILE of cavansite at 542 K.

```
# from D:/armbruster/cava265/CAVANSITE542K
_audit_creation_date          2015-06-29T15:46:59
_symmetry_space_group_name_H-M     'P nma'
_cell_length_a     9.6191(4)
_cell_length_b     13.6202(5)
_cell_length_c     9.7091(4)
_cell_angle_alpha     90.0000
_cell_angle_beta     90.0000
_cell_angle_gamma     90.0000
loop_
 _atom_site_label
 _atom_site_type_symbol
 _atom_site_fract_x
 _atom_site_fract_y
 _atom_site_fract_z
 _atom_site_B_iso_or_equiv
 _atom_site_occupancy
V V 0.0237(5) 0.25000 0.0918(6) 2.16(19) 1.00000
Ca CA -0.3783(7) 0.75000 -0.0876(8) 2.65(23) 1.00000
Si1 SI -0.1890(8) 0.5331(4) -0.0901(7) 2.34(13) 1.00000
Si2 SI -0.1055(7) 0.4535(5) 0.1898(7) 2.30(13) 1.00000
O1 O -0.1739(7) 0.6504(4) -0.0923(15) 2.43(16) 1.00000
O2 O -0.0845(13) 0.3380(5) 0.2138(10) 2.62(16) 1.00000
O3 O -0.1987(11) 0.4808(10) 0.0580(8) 2.67(16) 1.00000
O4 O -0.0454(8) 0.4999(7) -0.1609(12) 2.39(16) 1.00000
O5 O -0.3153(11) 0.4945(7) -0.1838(10) 2.31(16) 1.00000
O6 O -0.0405(18) 0.25000 -0.0591(10) 3.87(16) 1.00000
O7 O -0.4308(26) 0.8459(20) 0.1186(28) 11.56(18) 0.607(20)
O8 O -0.6146(29) 0.75000 -0.0486(26) 12.51(14) 1.00000
```

CIF FILE of cavansite at 783 K.

```
# from D:/armbruster/cava510/CAVANSITE783K
_audit_creation_date            2015-06-29T15:48:02
_symmetry_space_group_name_H-M     'P n m a'
_cell_length_a     9.4826(15)
_cell_length_b     13.3074(20)
_cell_length_c     9.4864(25)
_cell_angle_alpha     90.0000
_cell_angle_beta     90.0000
_cell_angle_gamma     90.0000
loop_
 _atom_site_label
 _atom_site_type_symbol
 _atom_site_fract_x
 _atom_site_fract_y
 _atom_site_fract_z
 _atom_site_B_iso_or_equiv
 _atom_site_occupancy
V V 0.0270(15) 0.25000 0.0834(17) 2.5(6) 1.00000
Ca CA -0.3872(28) 0.75000 -0.0852(27) 5.5(9) 1.00000
Si1 SI -0.1884(24) 0.5344(15) -0.0826(24) 4.0(6) 1.00000
Si2 SI -0.0941(20) 0.4593(13) 0.2110(29) 3.9(6) 1.00000
O1 O -0.1853(20) 0.6540(15) -0.0623(37) 6.2(7) 1.00000
O2 O -0.0692(45) 0.3403(14) 0.2187(26) 6.4(7) 1.00000
O3 O -0.1848(45) 0.4899(33) 0.0747(24) 6.4(7) 1.00000
O4 O -0.0576(22) 0.4941(18) -0.1740(44) 6.1(7) 1.00000
O5 O -0.3322(30) 0.4939(21) -0.1515(28) 6.1(7) 1.00000
O6 O -0.0536(57) 0.25000 -0.0635(28) 7.6(7) 1.00000
O8 O -0.5855(111) 0.75000 0.0811(114) 16.15(18) 0.695(50)
```